Supporting Information

Design, Synthesis and Biological Evaluations of Asymmetric Bow-Tie PAMAM Dendrimer-Based Conjugates for Tumor-Targeted Drug Delivery

Tao Wang,[†] Yaozhong Zhang,[†] Longfei Wei,[†] Yuhan G. Teng,[†] Tadashi Honda[†,‡] and Iwao Ojima*[,†,‡]

† Department of Chemistry and ‡ Institute of Chemical Biology and Drug Discovery, Stony Brook University, Stony Brook, New York 11794-3400, U. S. A.

*Corresponding author: E-mail iwao.ojima@stonybrook.edu

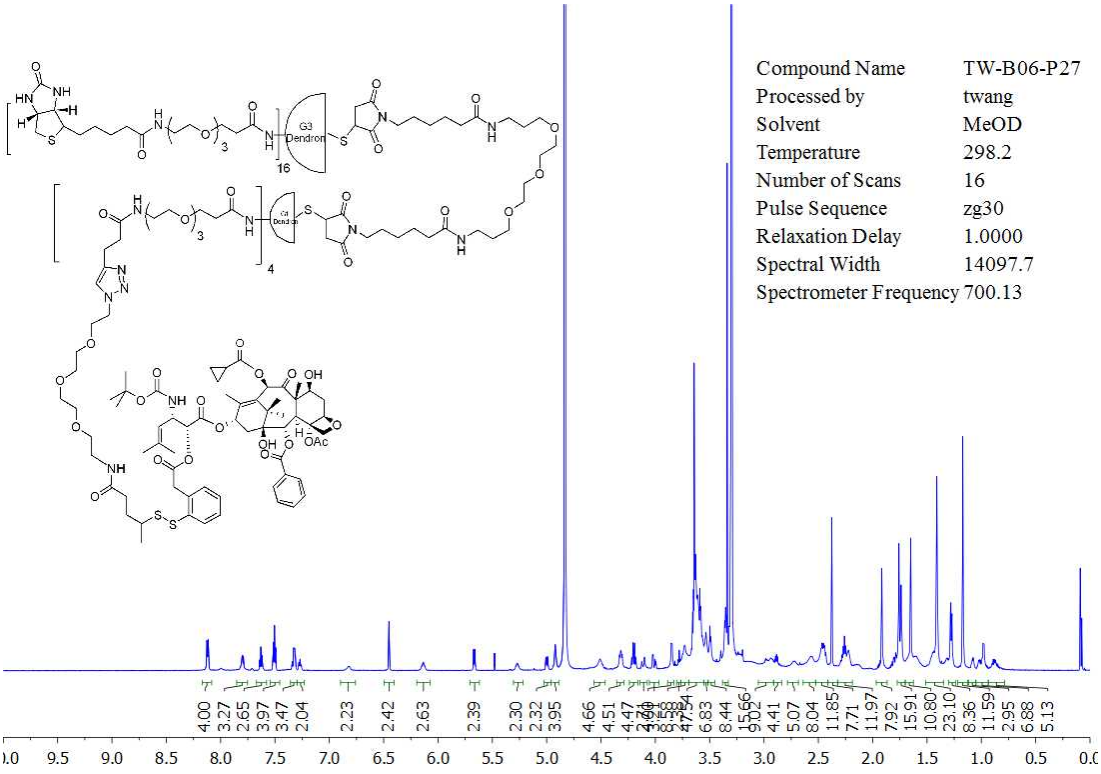

Figure S1. ^{1}H NMR spectrum of **1**

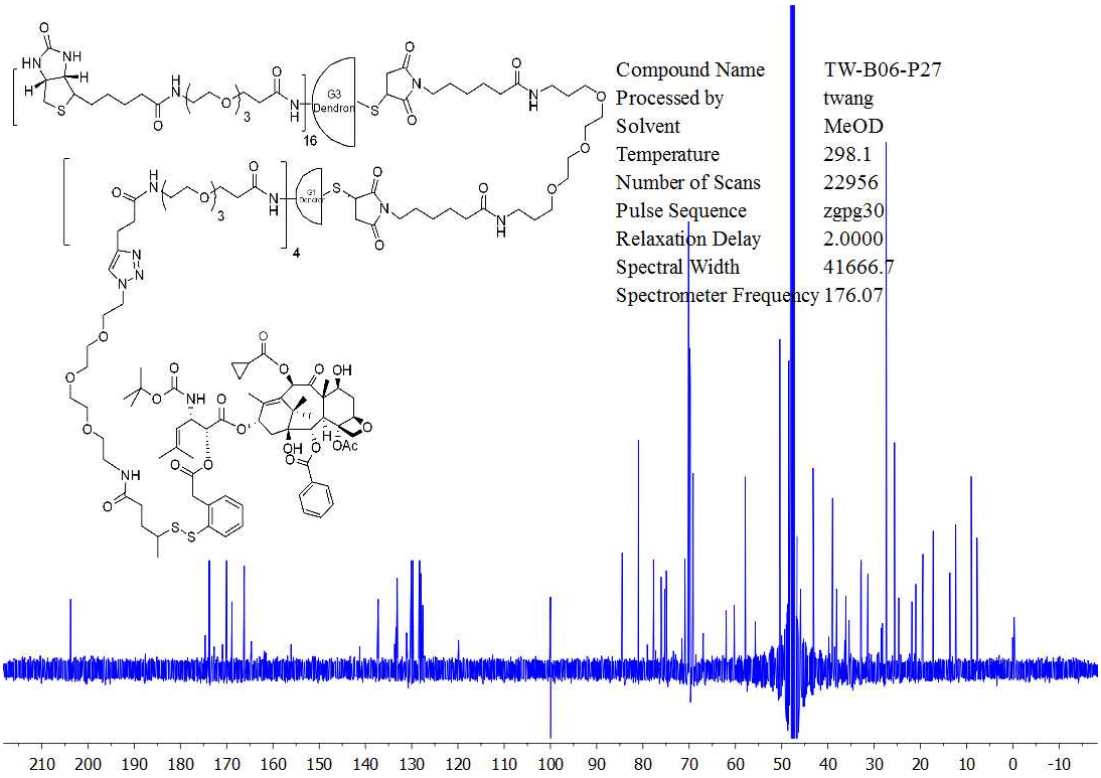

Figure S2. ^{13}C NMR spectrum of **1**

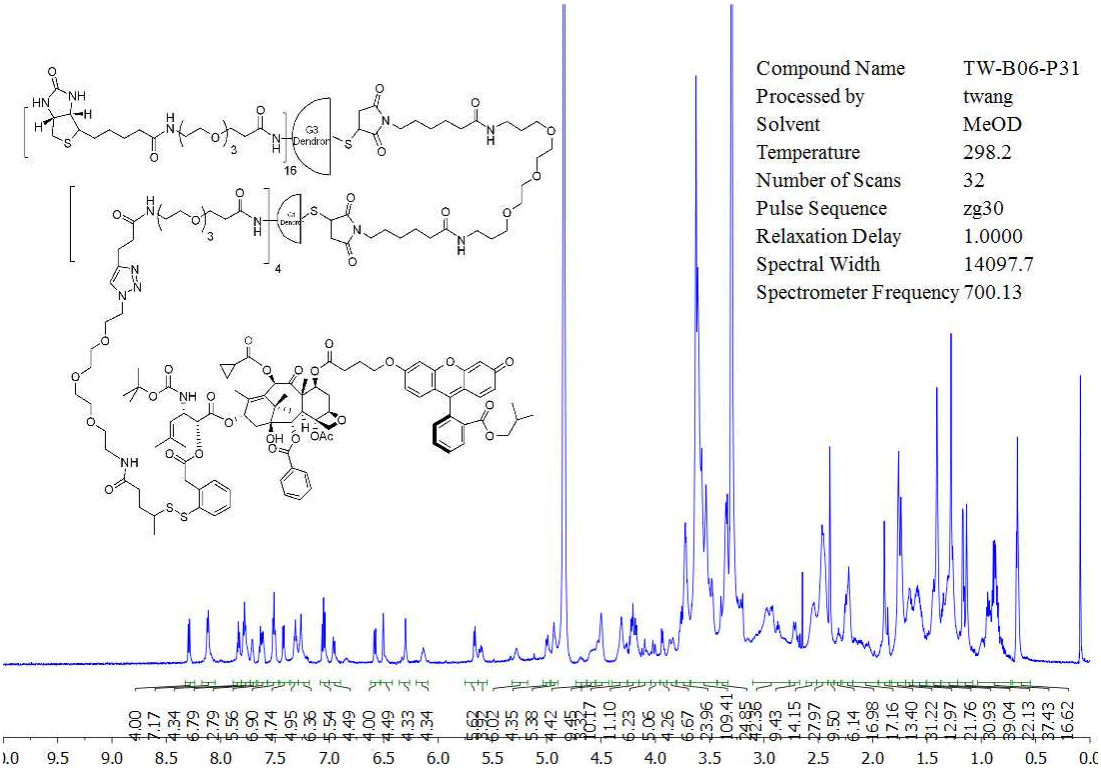

Figure S3. ^{1}H NMR spectrum of **2**

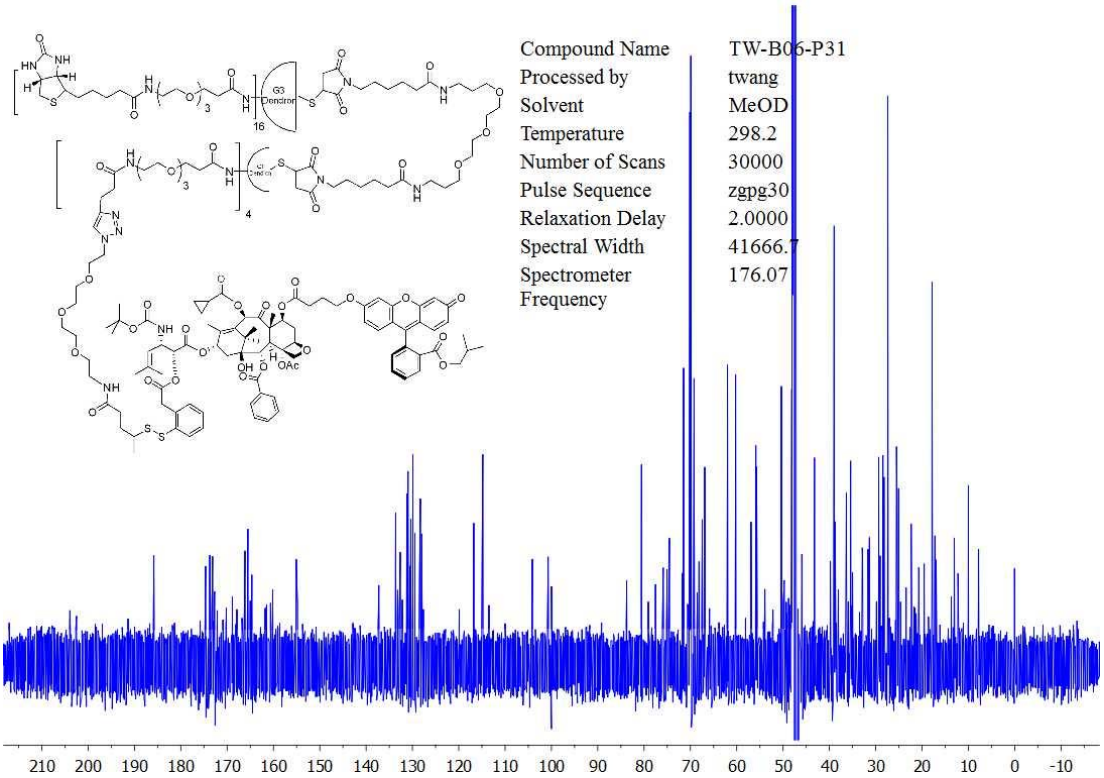

Figure S4. ^{13}C NMR spectrum of **2**

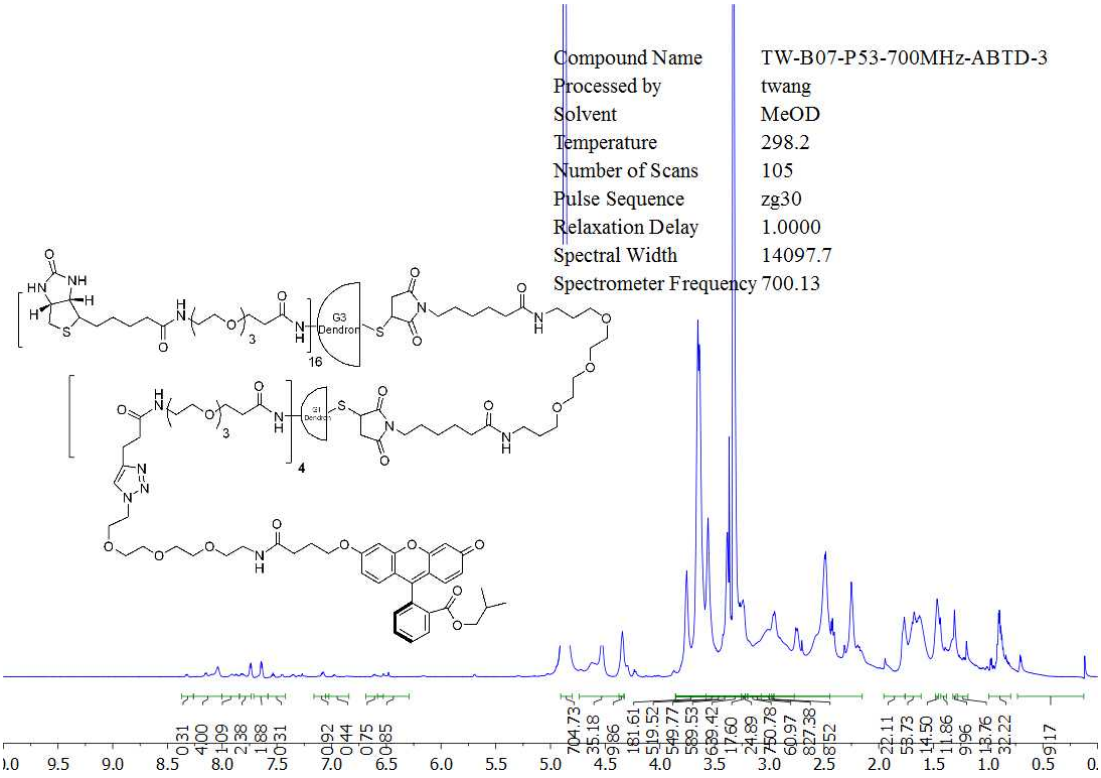

Figure S5. ^{1}H NMR spectrum of **3**

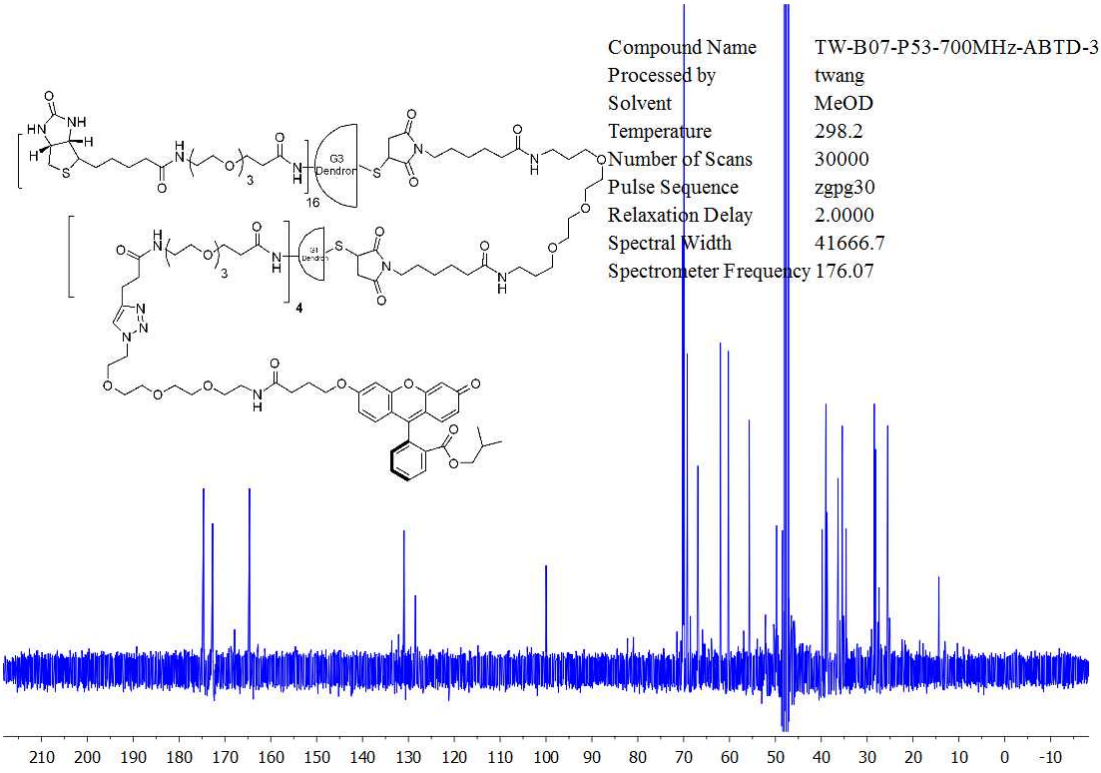

Figure S6. ^{13}C NMR spectrum of **3**

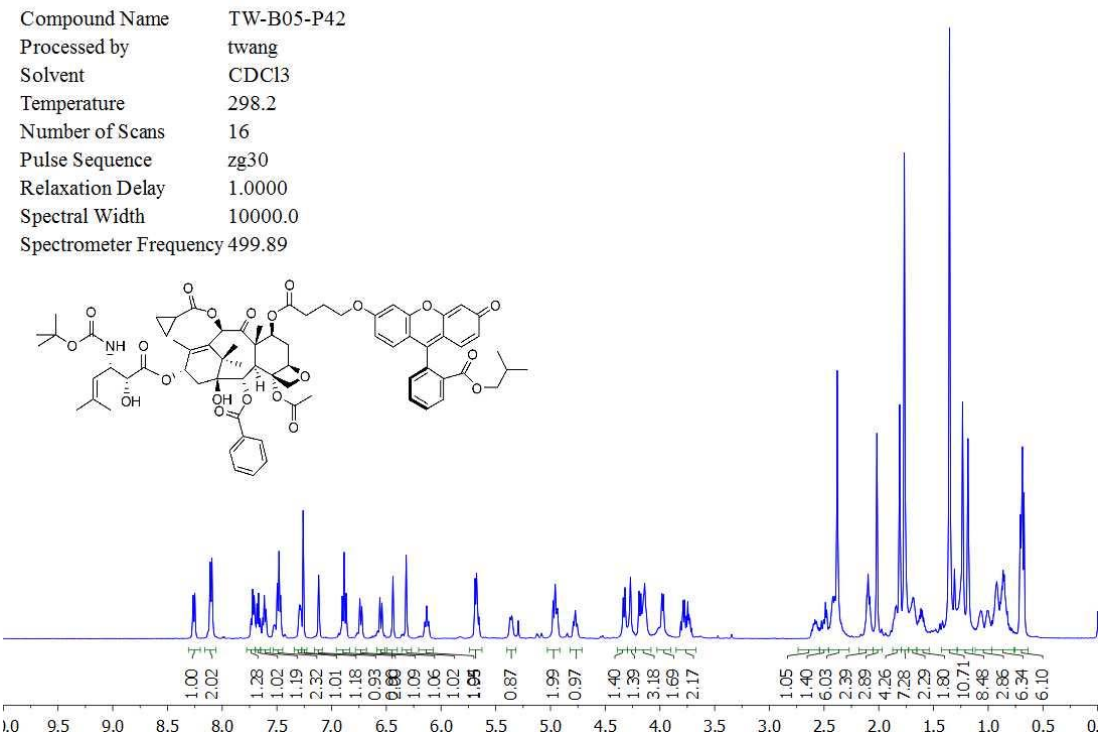

Figure S7. ^{1}H NMR spectrum of **5**

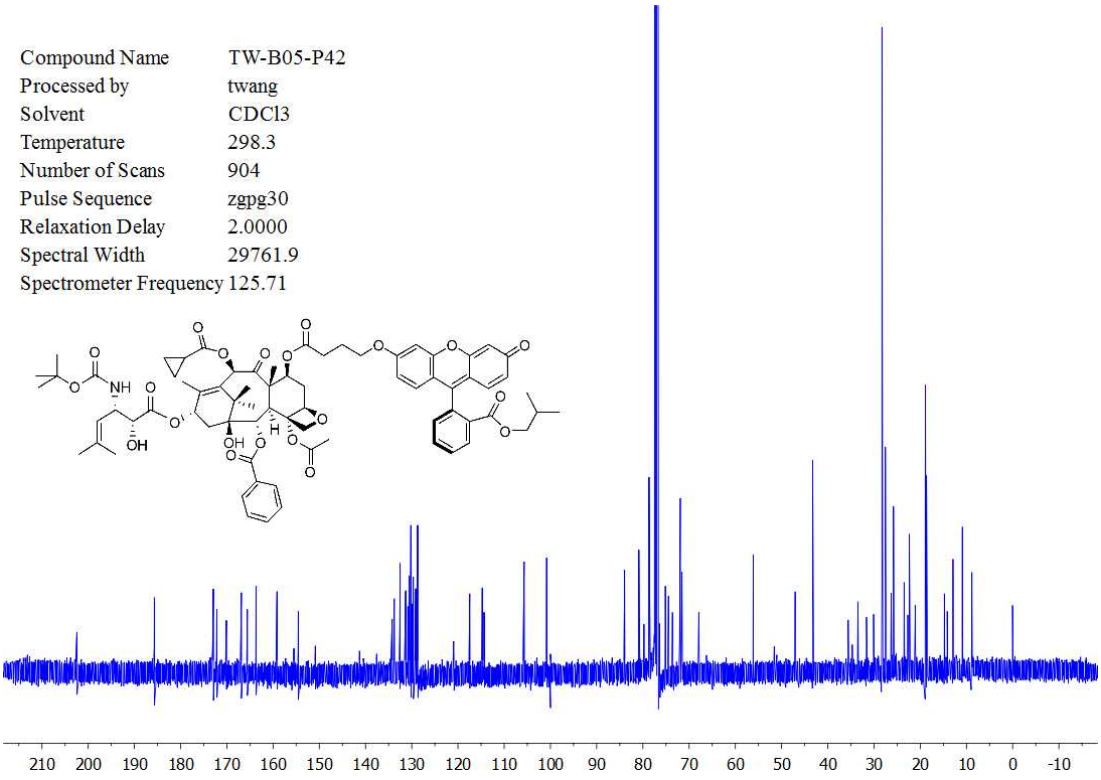

Figure S8. ^{13}C NMR spectrum of **5**

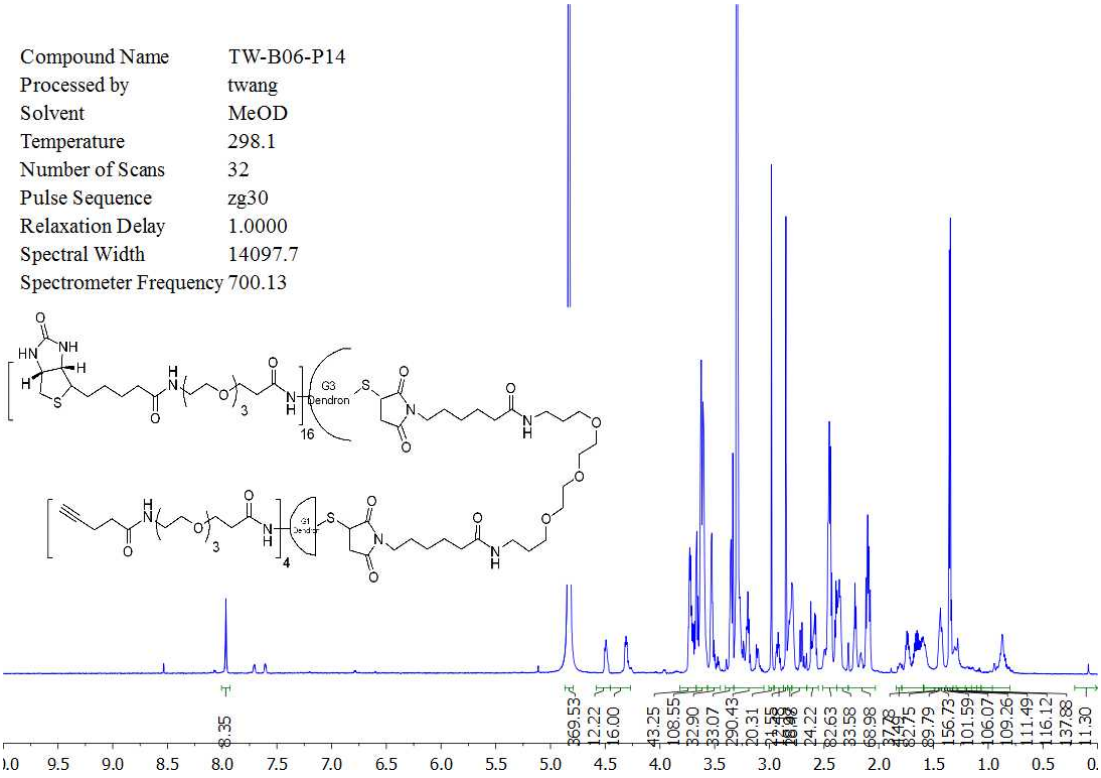

Figure S9. ^{1}H NMR spectrum of **6**

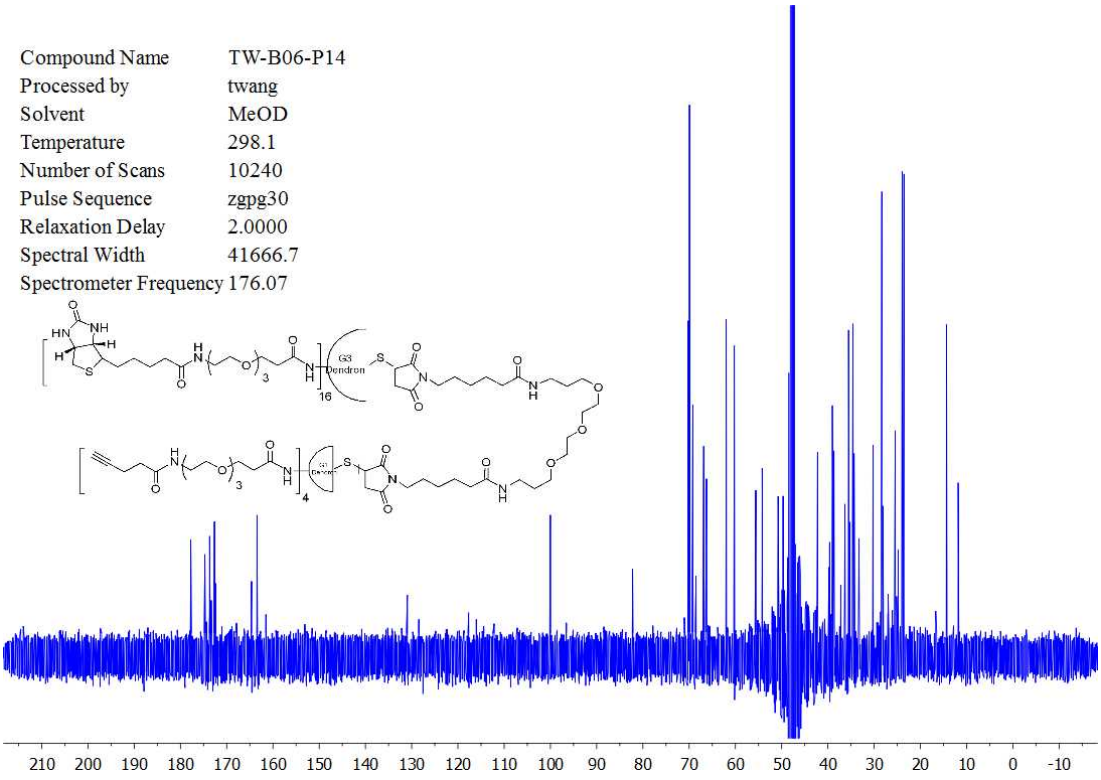

Figure S10. ^{13}C NMR spectrum of **6**

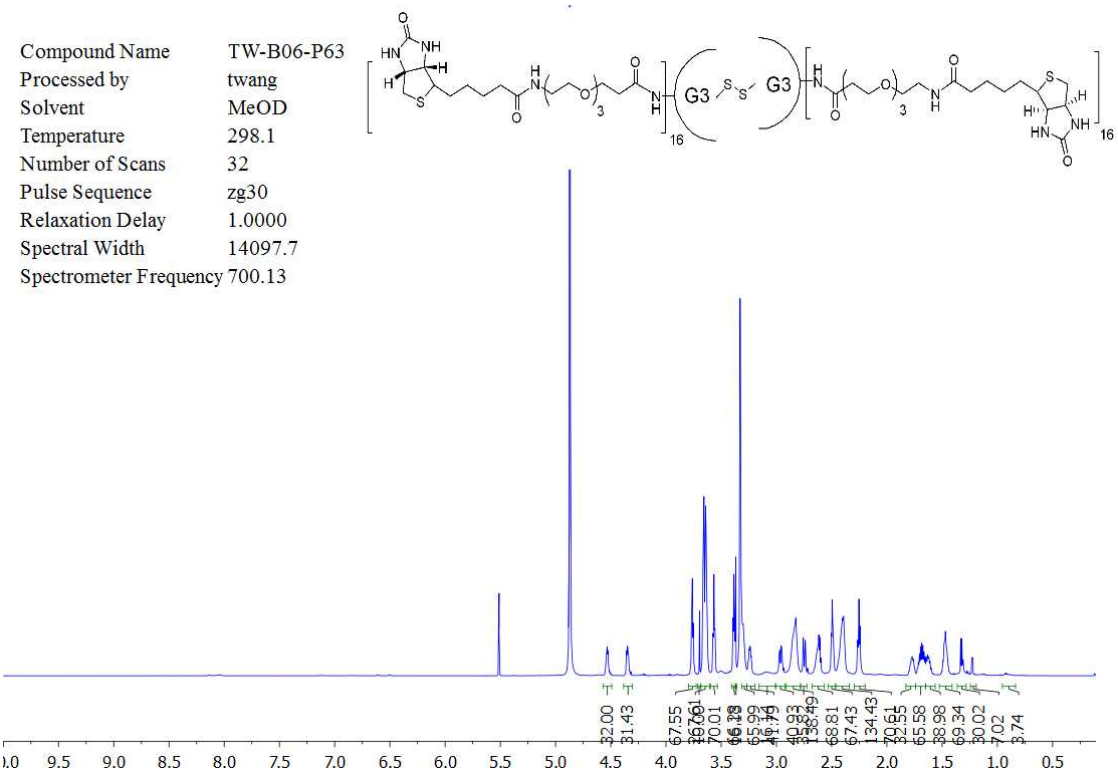

Figure S11. ^{1}H NMR spectrum of **7**

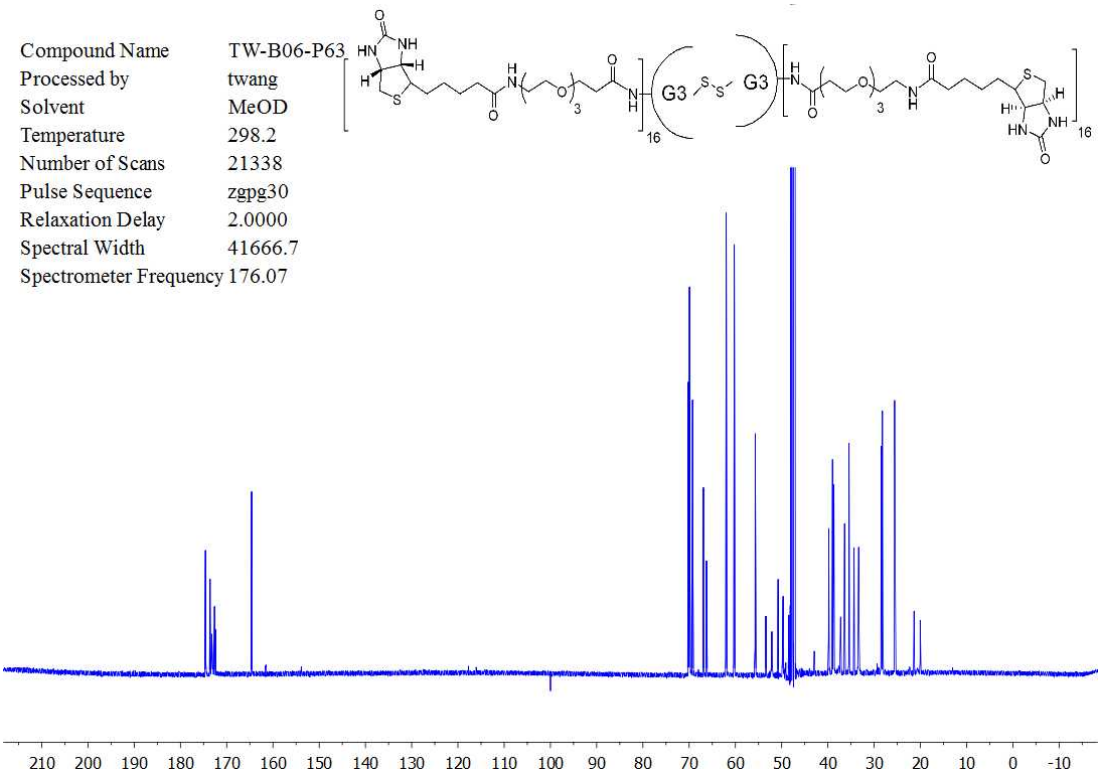

Figure S12. ^{13}C NMR spectrum of **7**

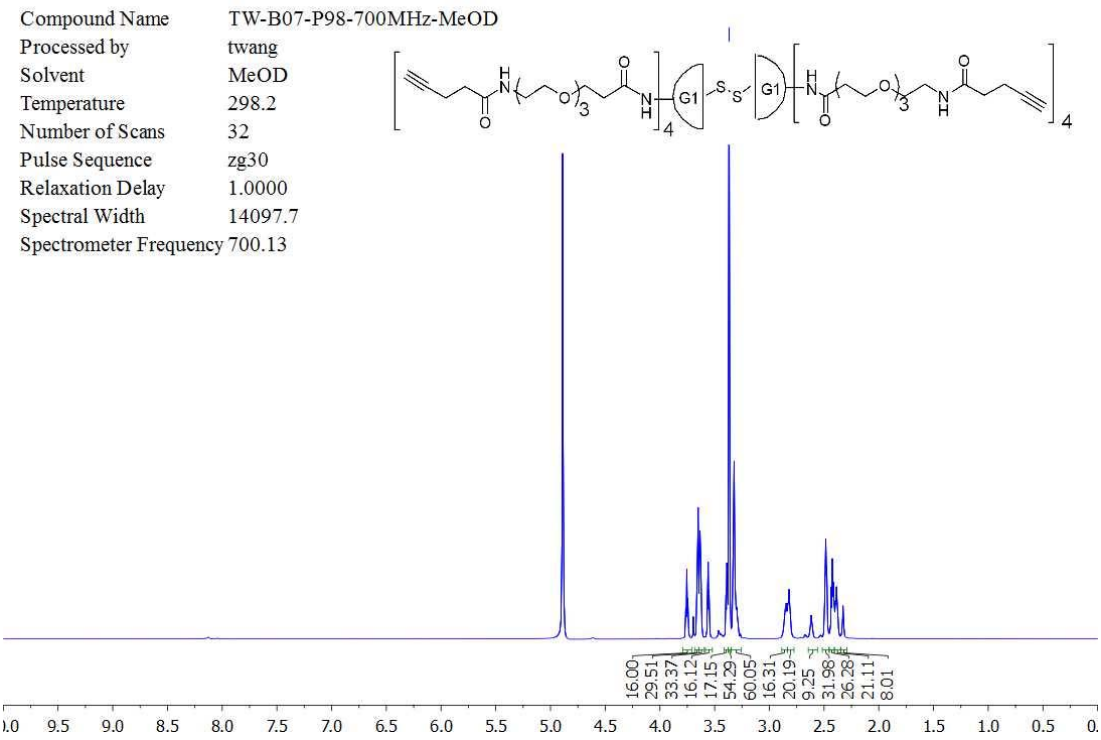

Figure 13. ^{1}H NMR spectrum of **8**

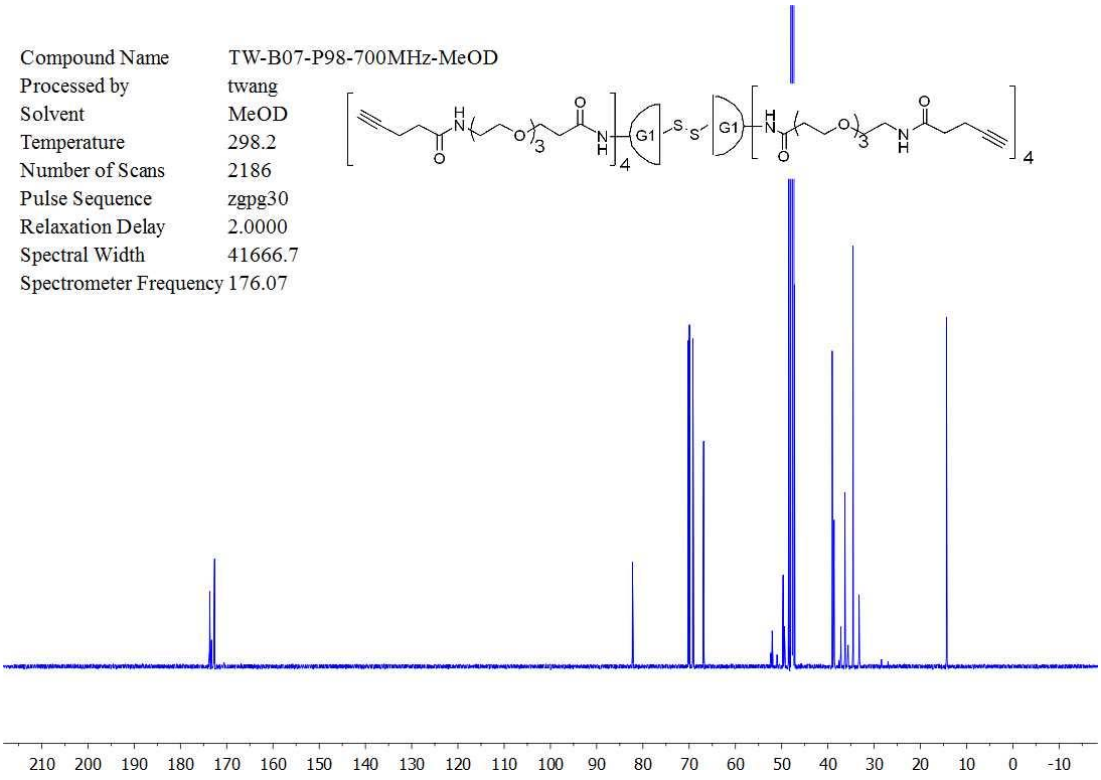

Figure S14. ^{13}C NMR spectrum of **8**

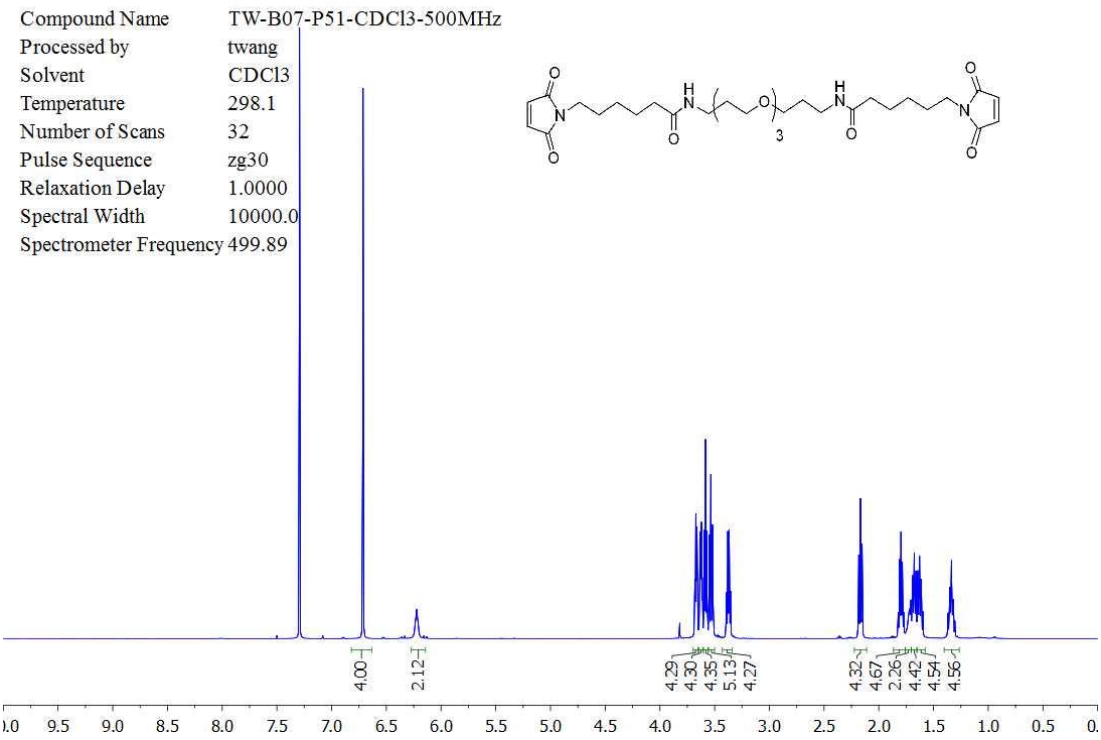

Figure S15. ^{1}H NMR spectrum of **9**

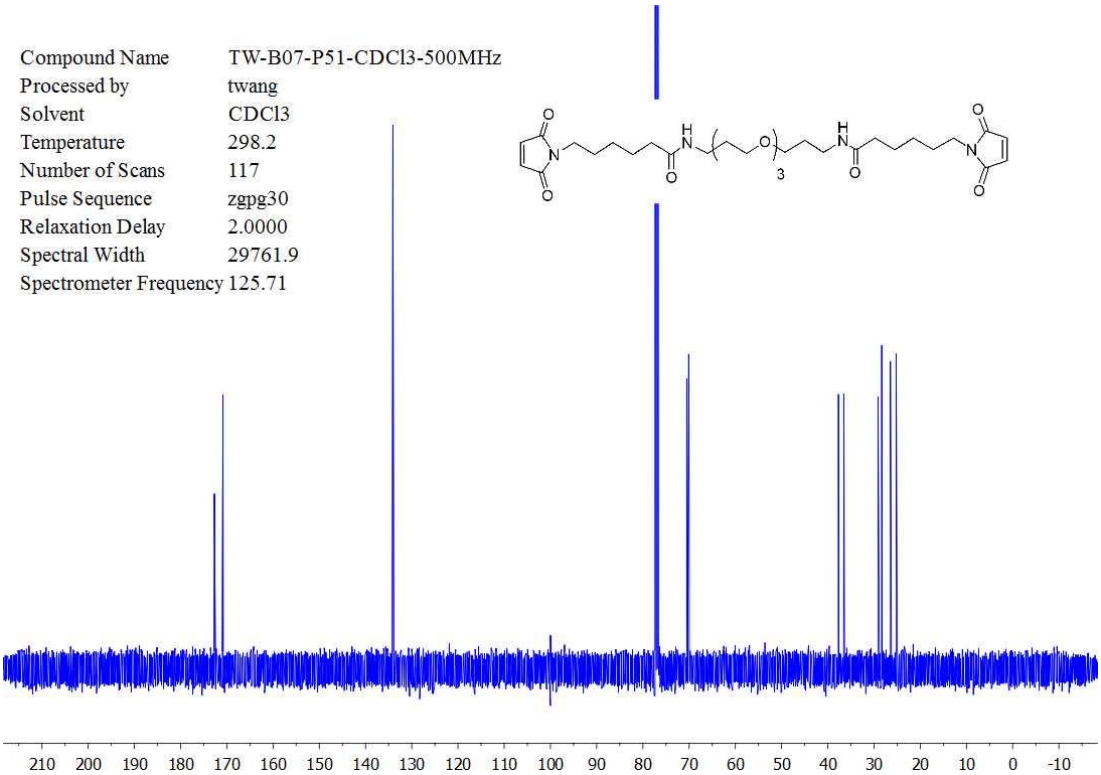

Figure S16. ^{13}C NMR spectrum of **9**

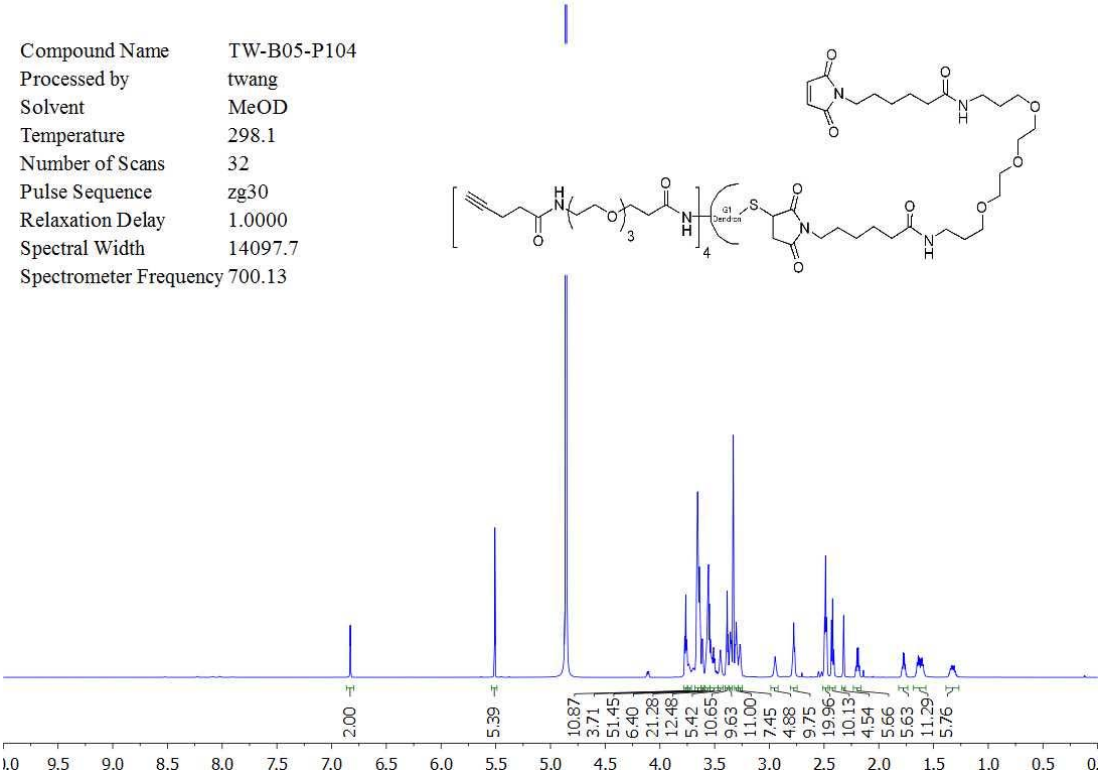

Figure S17. ^{1}H NMR spectrum of **12**

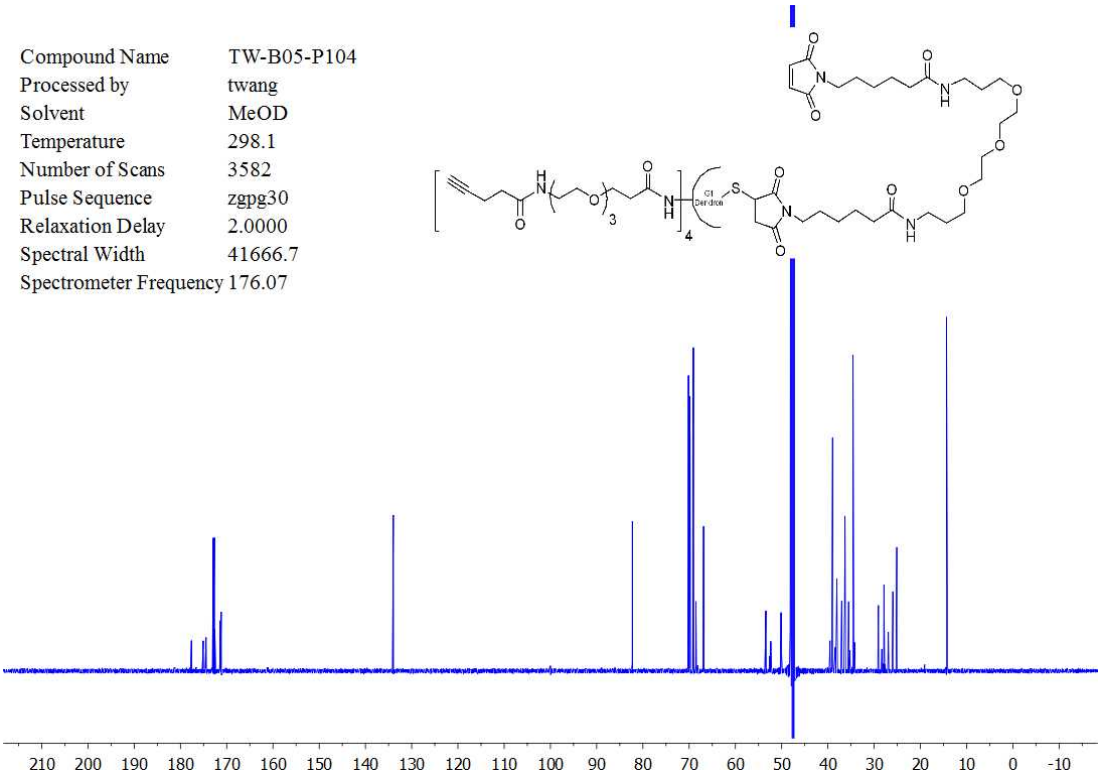

Figure S18. ^{13}C NMR spectrum of **12**

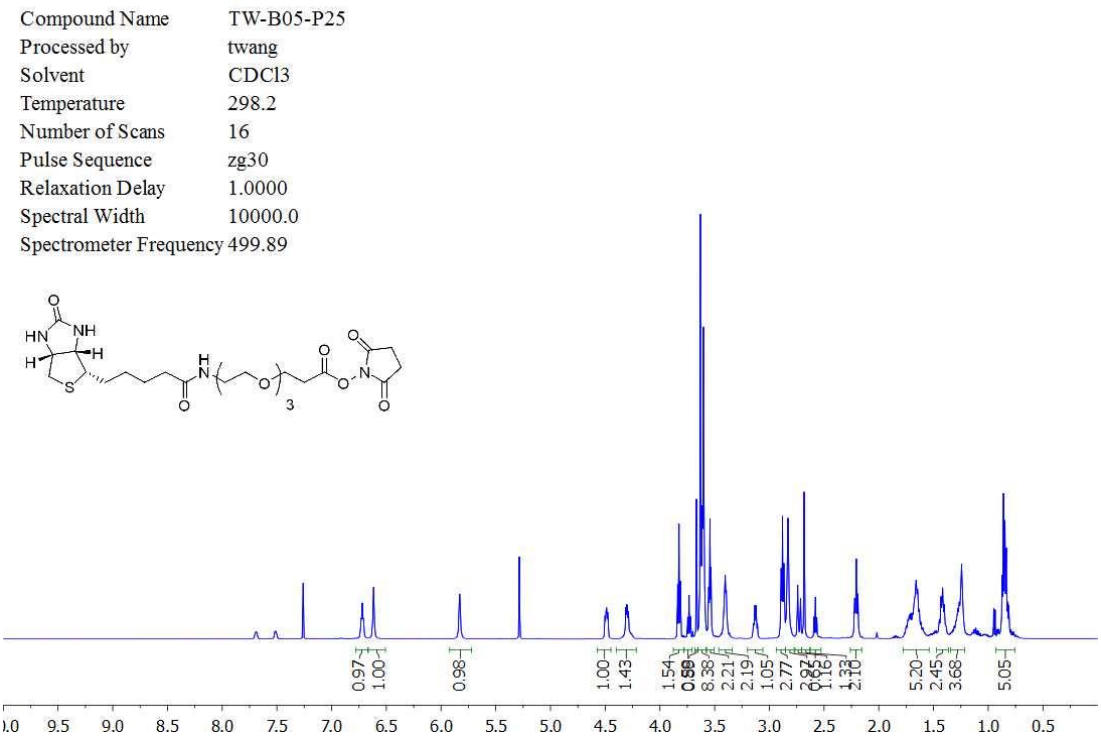

Figure S19. ^{1}H NMR spectrum of **14**

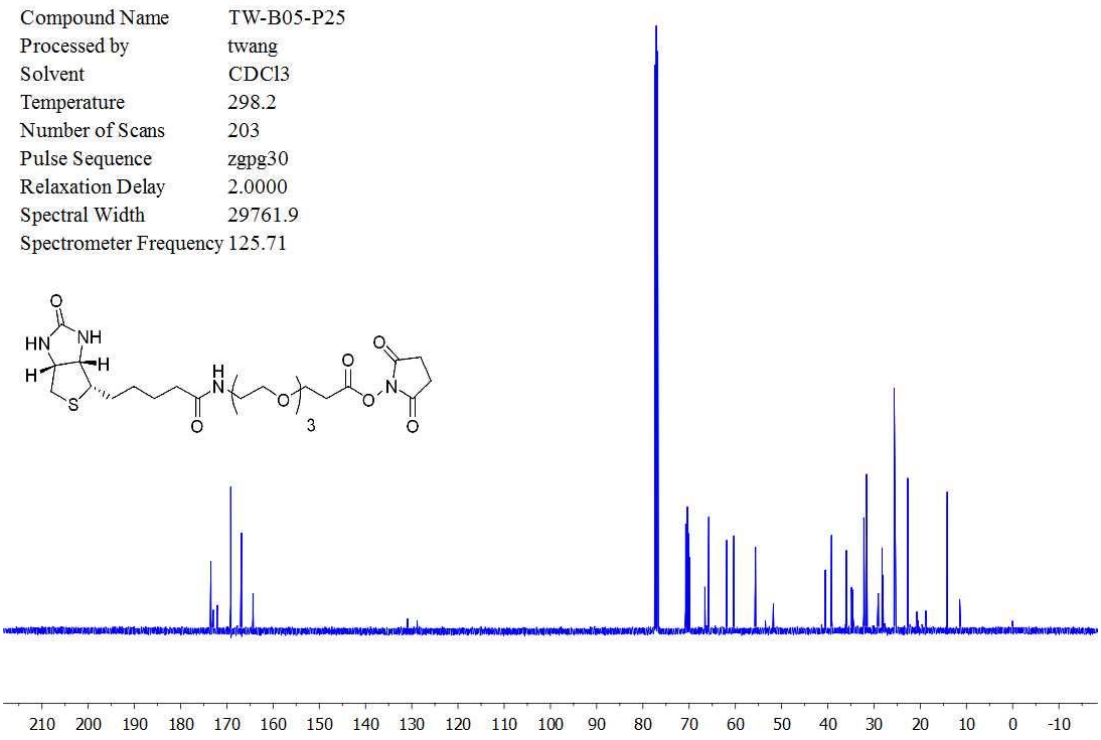

Figure S20. ^{13}C NMR spectrum of **14**

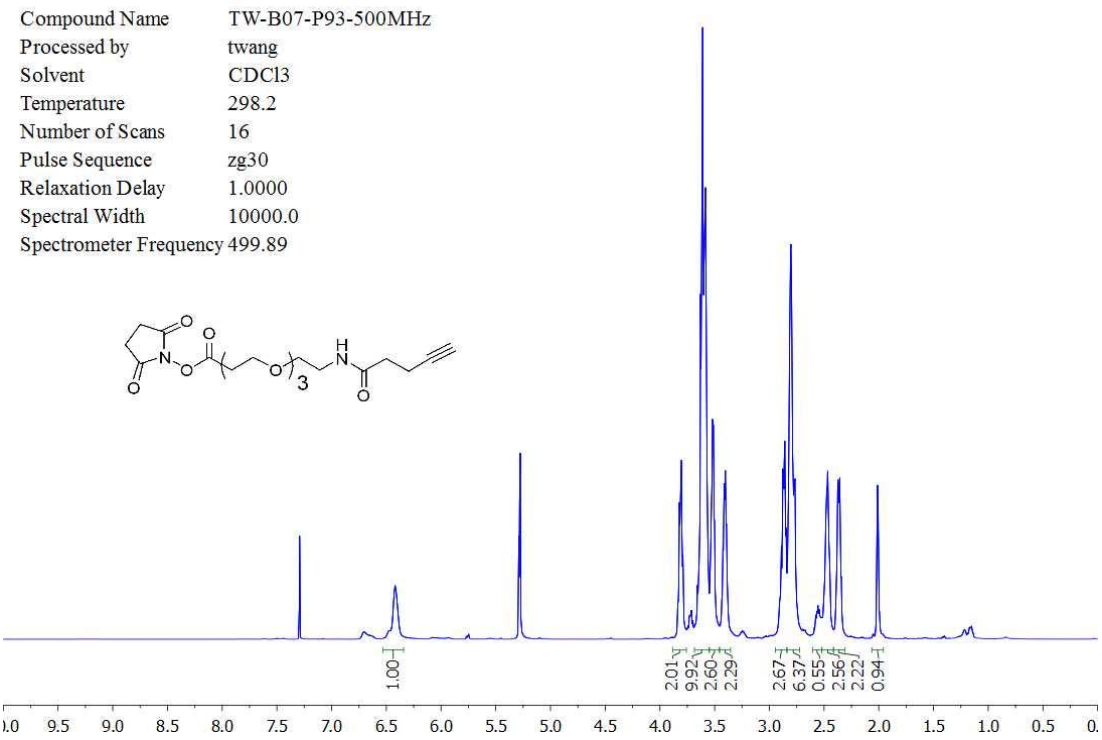

Figure S21 ^{1}H NMR spectrum of **16**

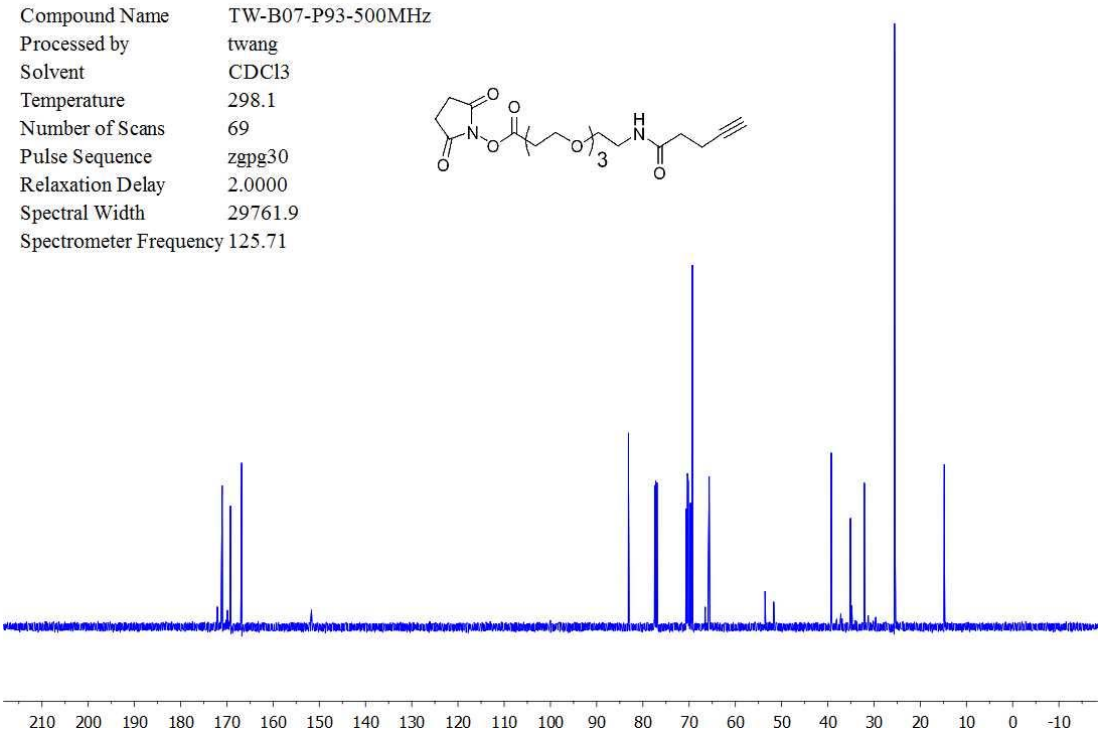

Figure S22. ^{13}C NMR spectrum of **16**

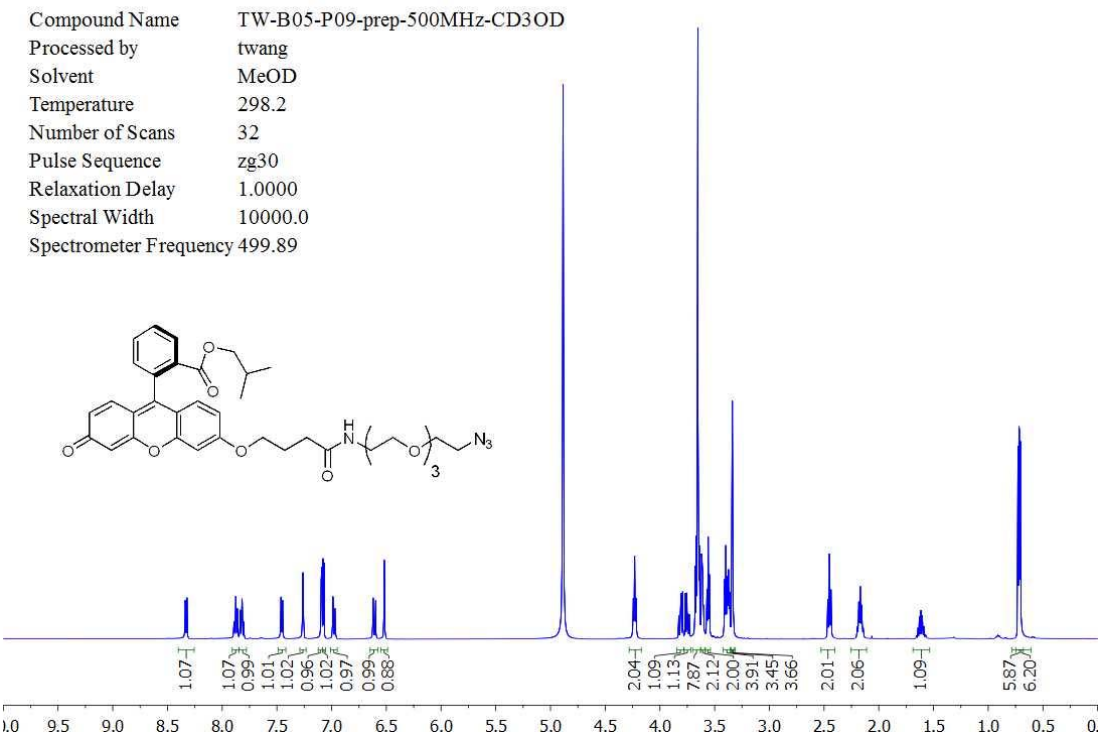

Figure S23. ^{1}H NMR spectrum of **19**

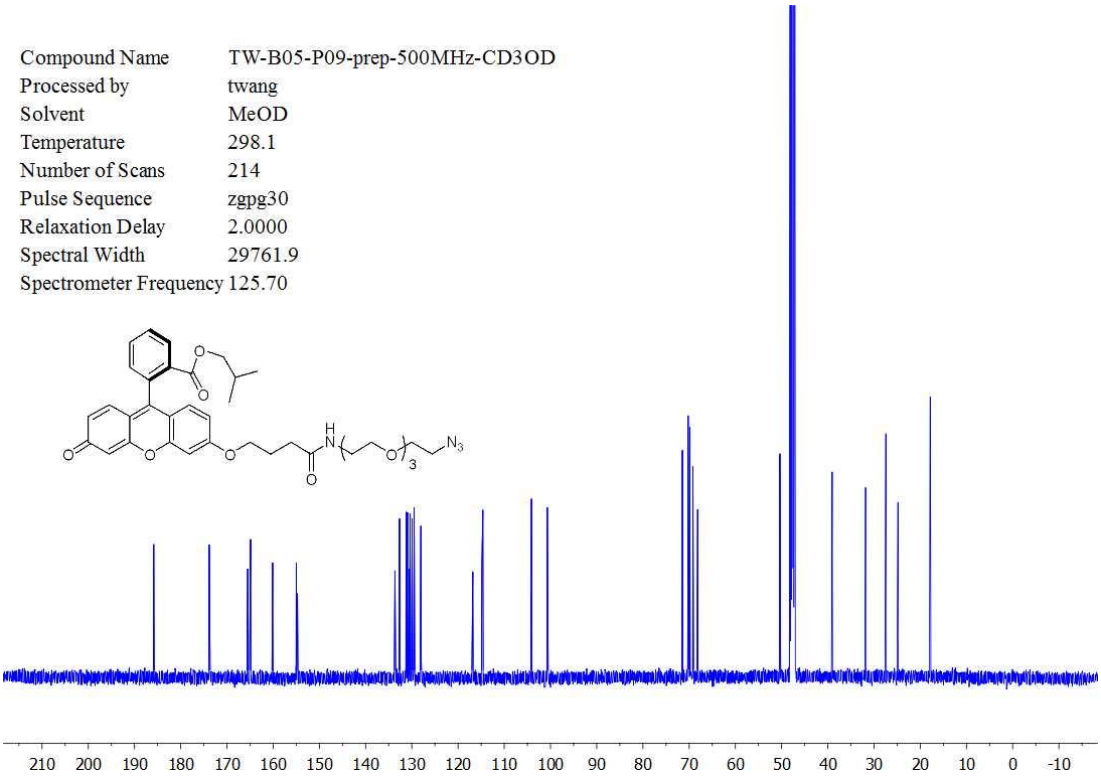

Figure S24. ^{13}C NMR spectrum of **19**

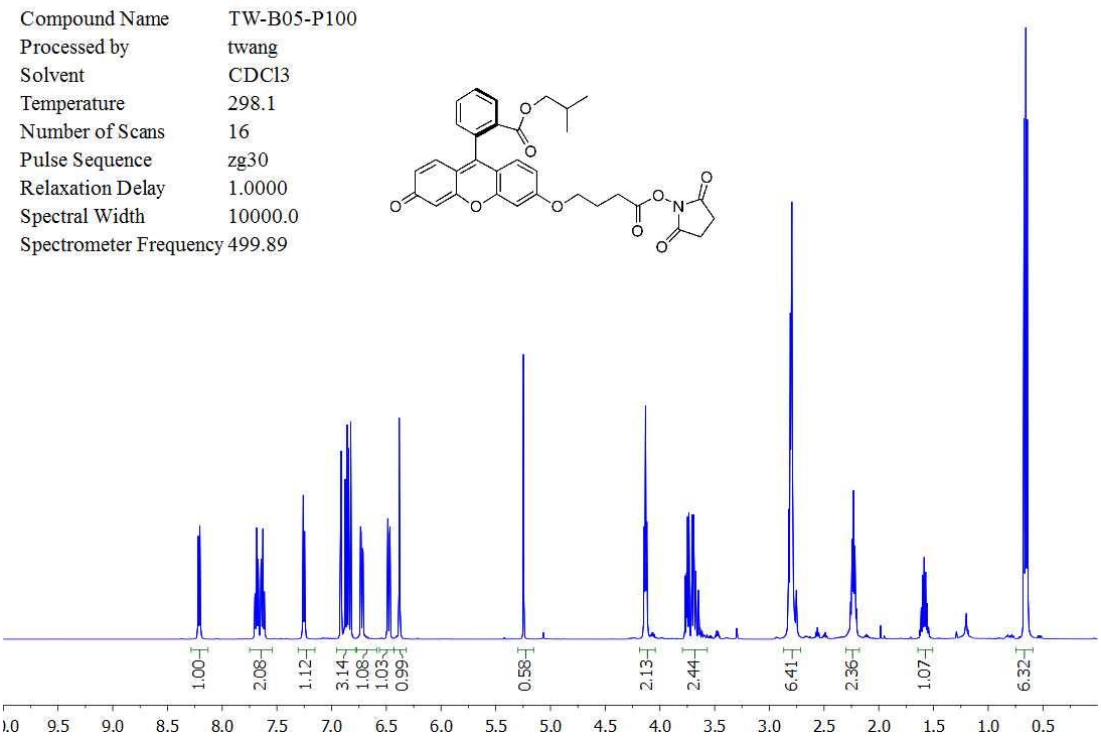

Figure S25. ^{1}H NMR spectrum of **20**

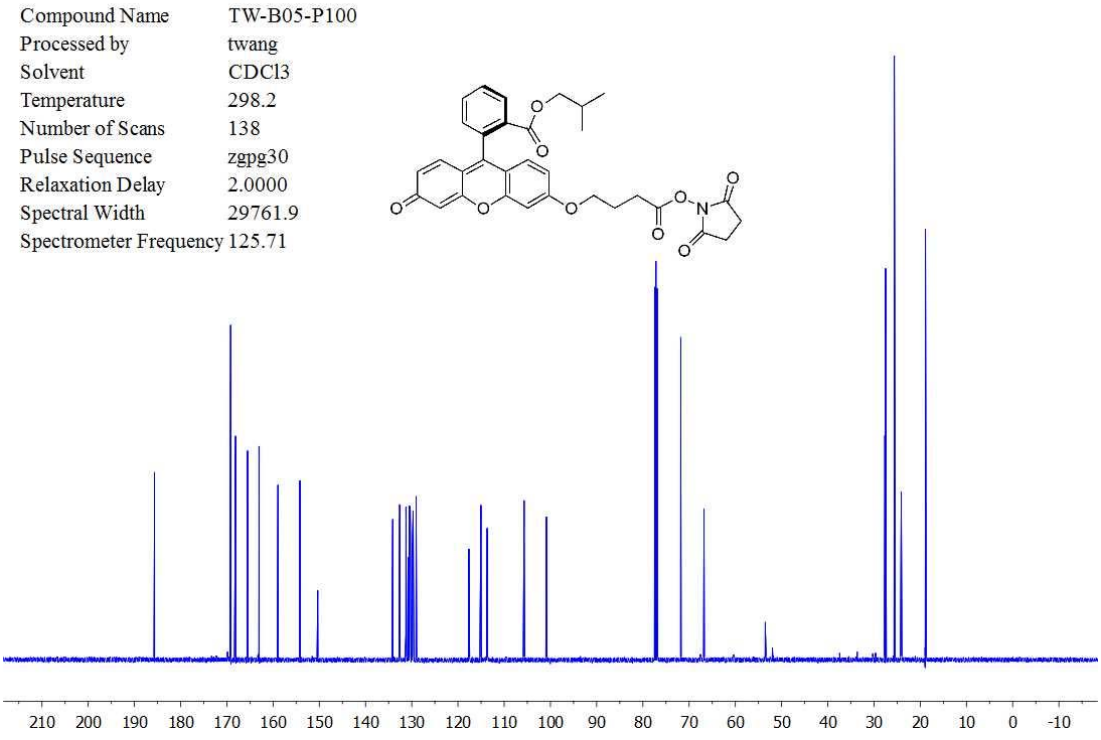

Figure S26. ^{13}C NMR spectrum of **20**

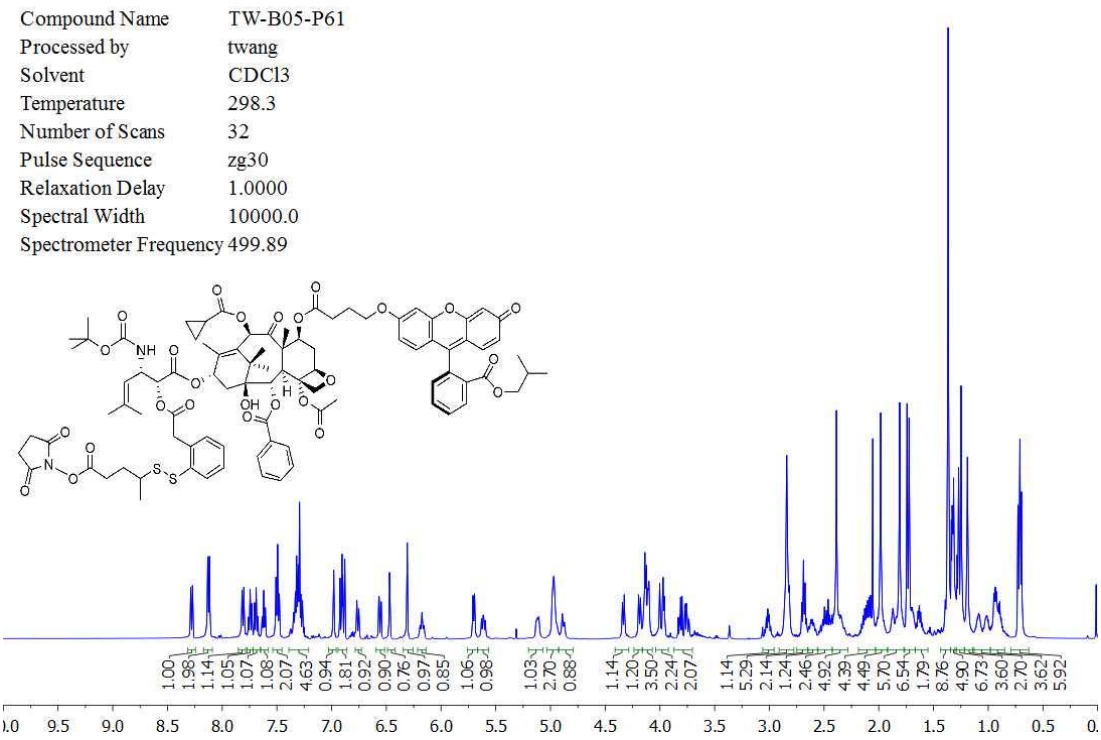

Figure S27. ^{1}H NMR spectrum of **22**

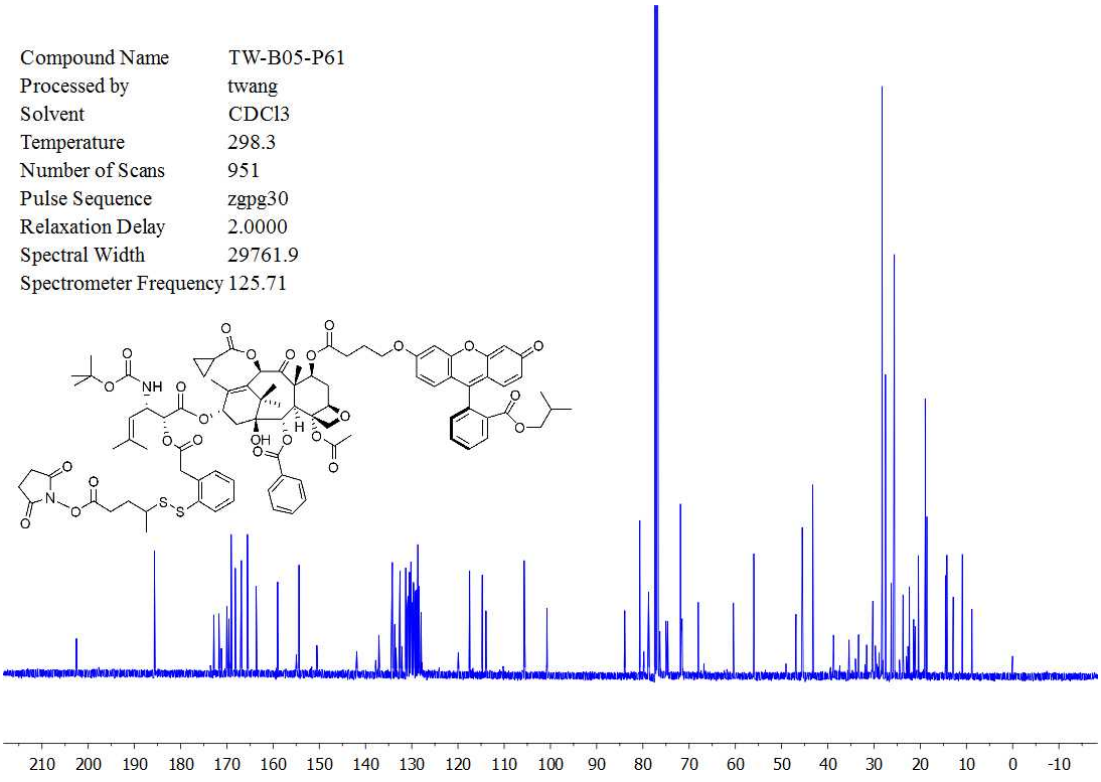

Figure S28. ^{13}C NMR spectrum of **22**

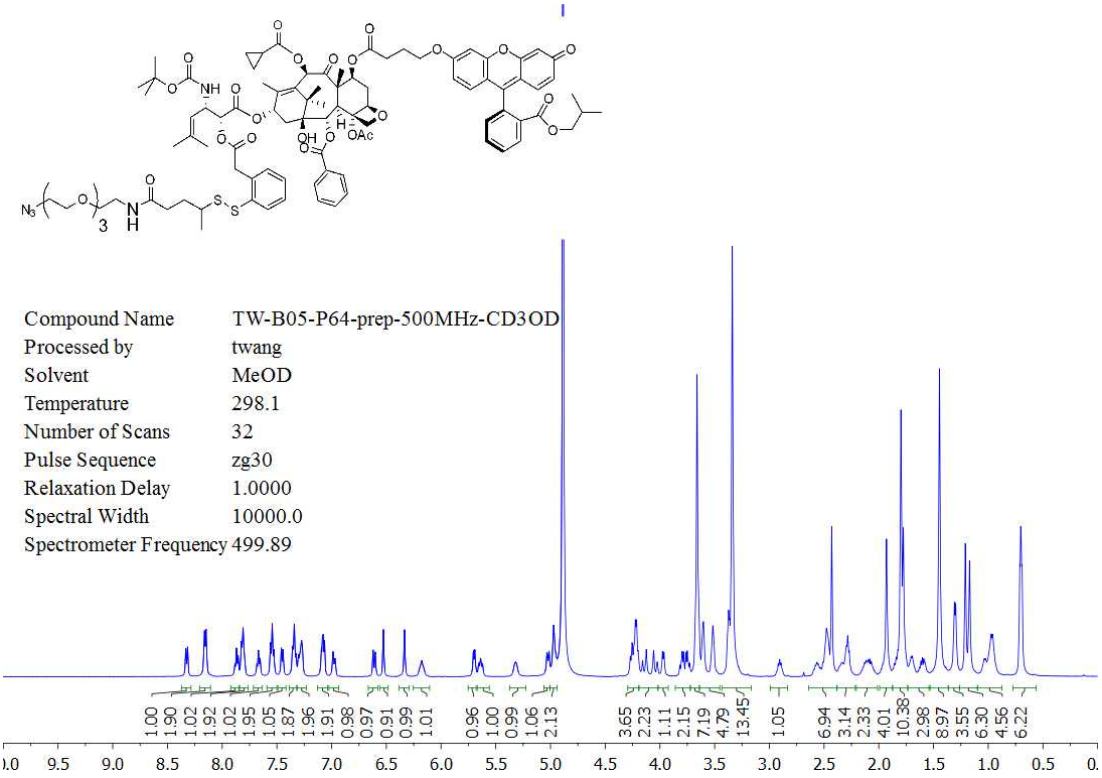

Figure S29. ^{1}H NMR spectrum of **24**

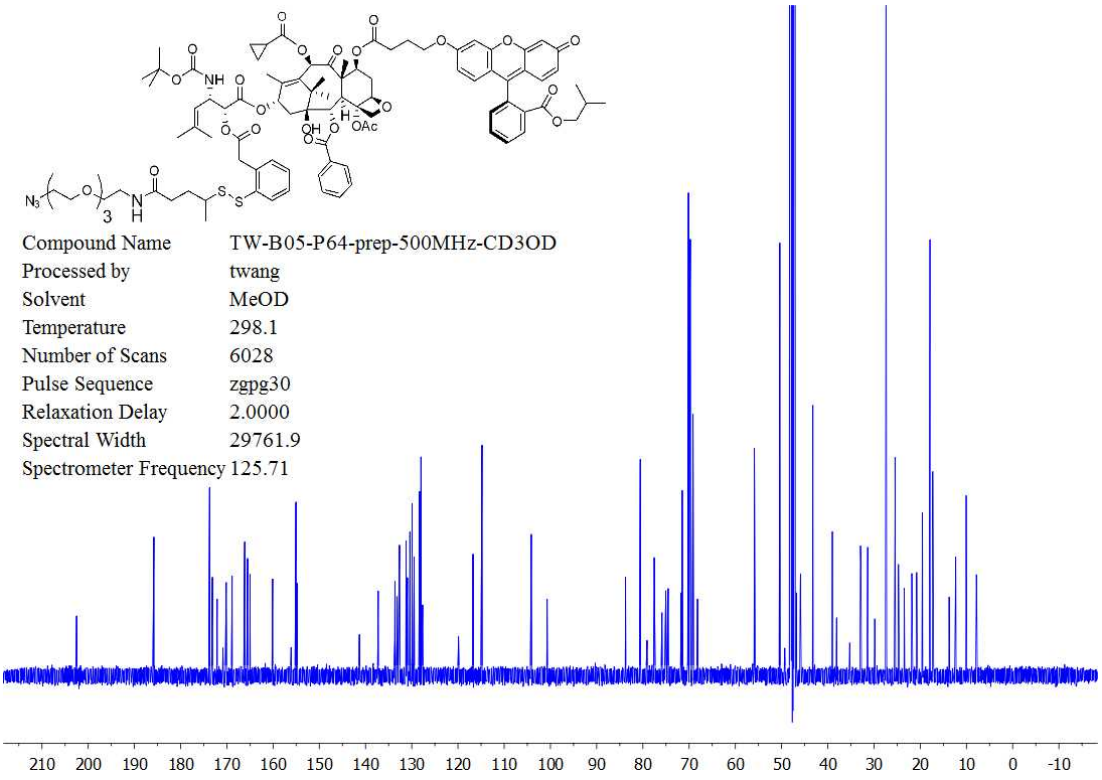

Figure S30. ^{13}C NMR spectrum of **24**

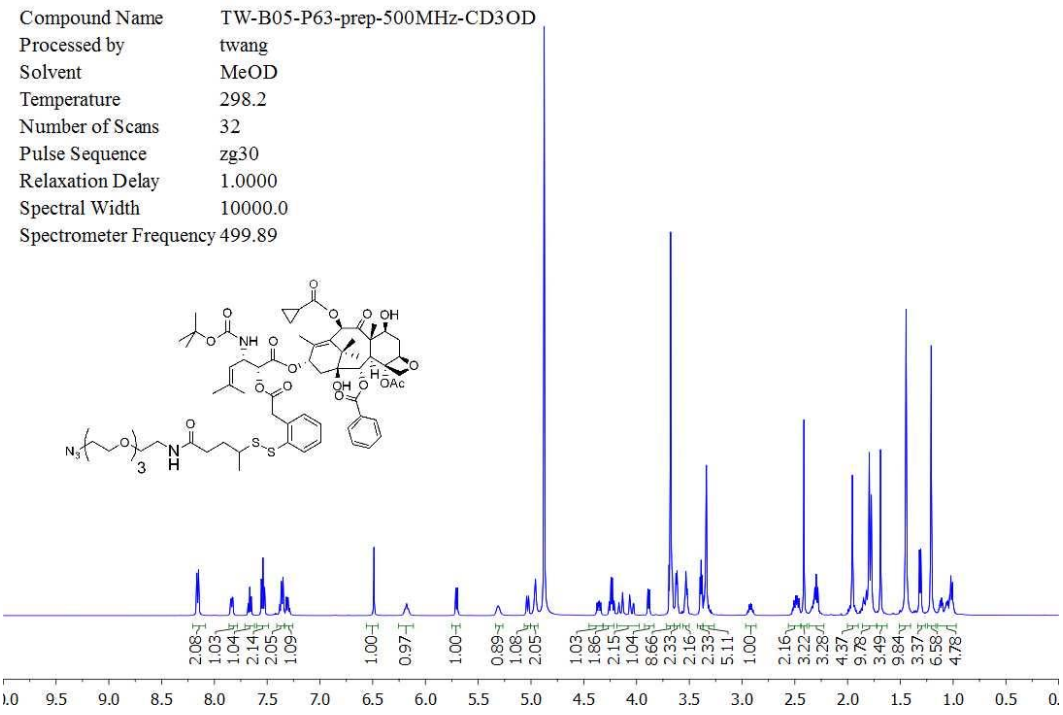

Figure S31. ^{1}H NMR spectrum of **25**

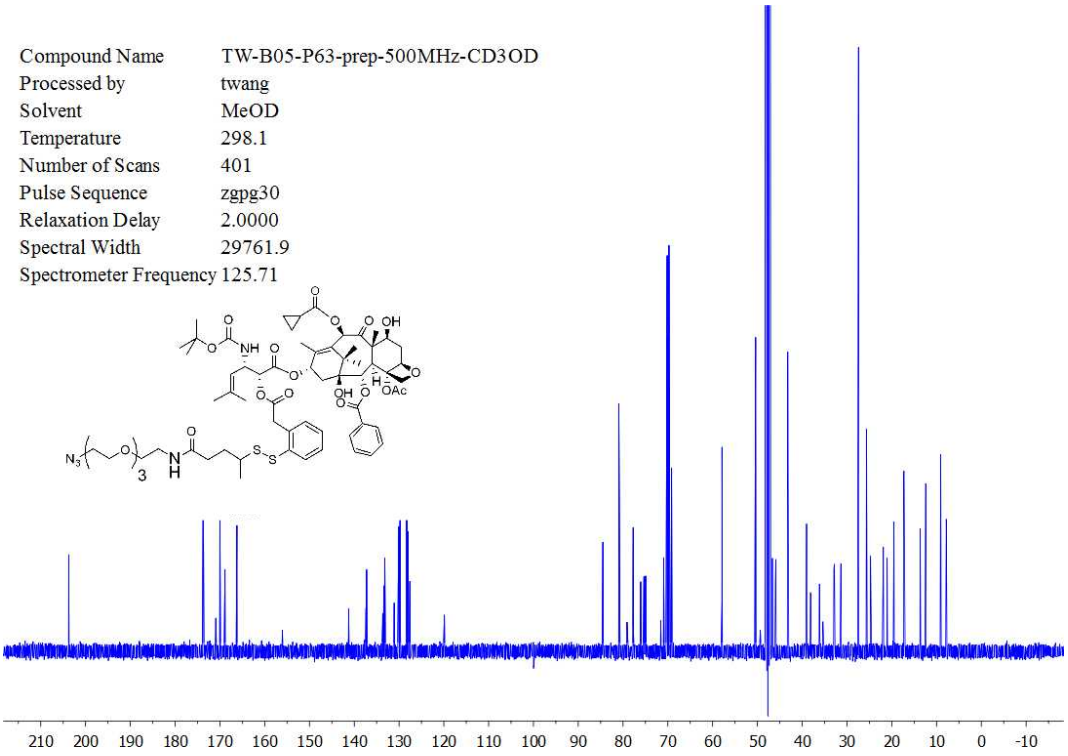

Figure S32. ^{13}C NMR spectrum of **25**

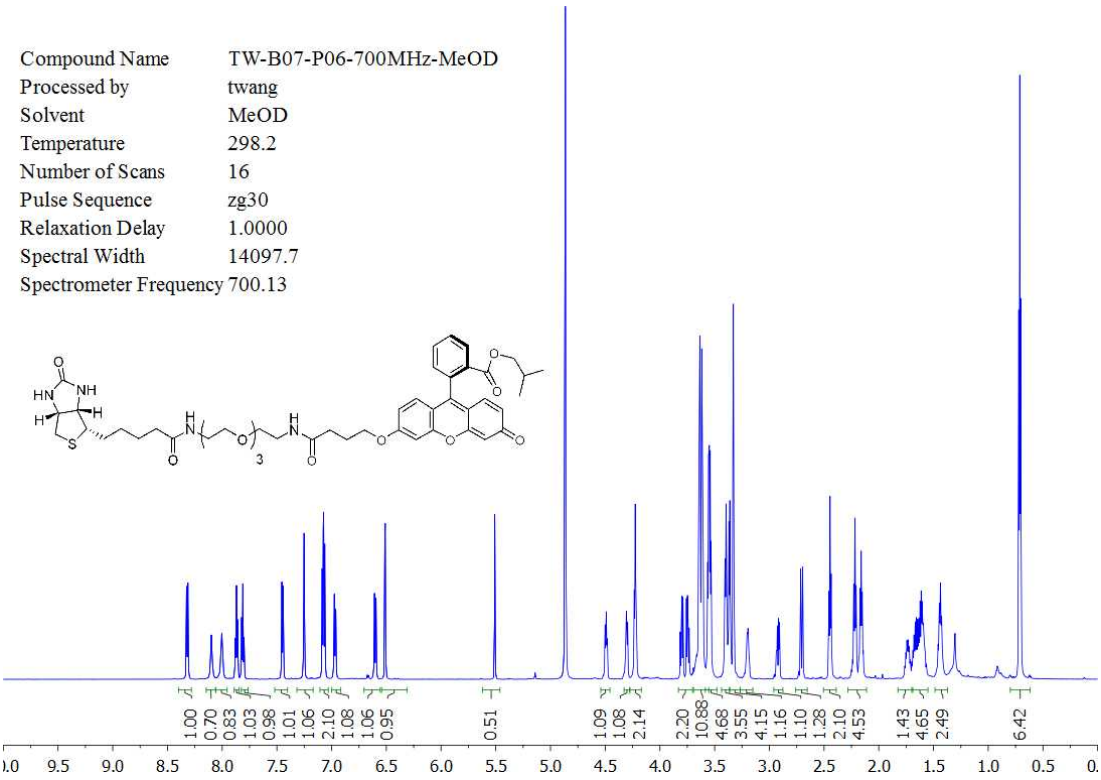

Figure S33. ^{1}H NMR spectrum of **28**

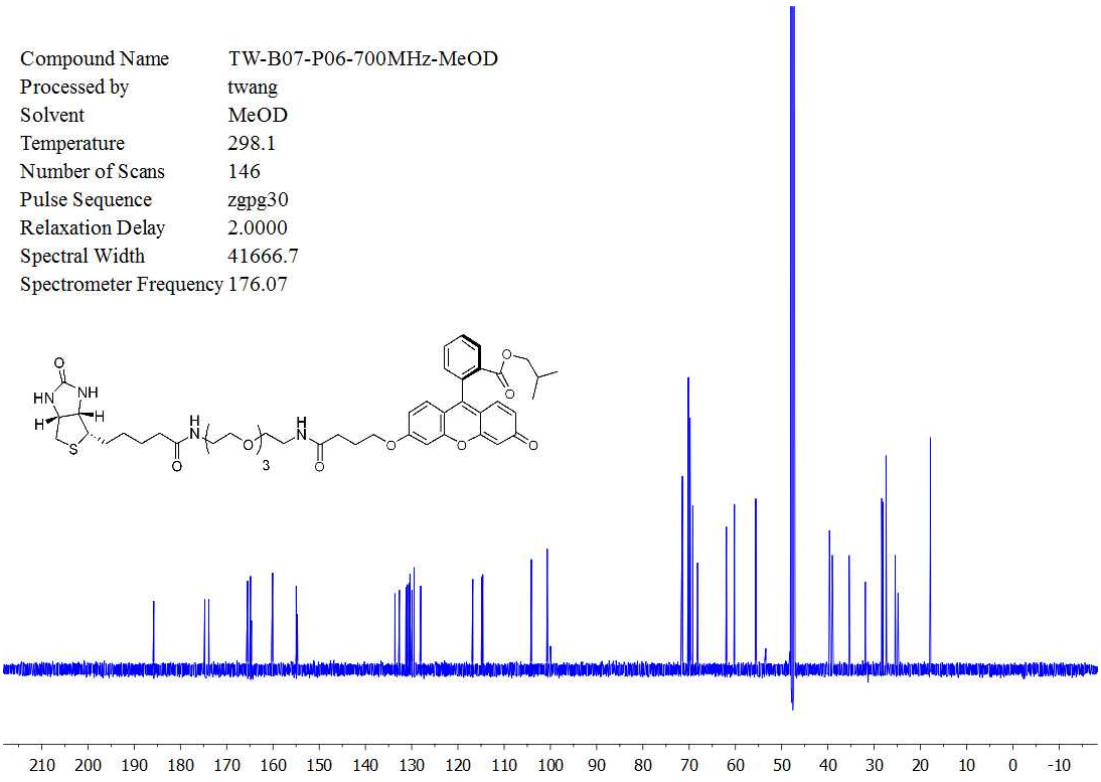

Figure S34. ^{13}C NMR spectrum of **28**

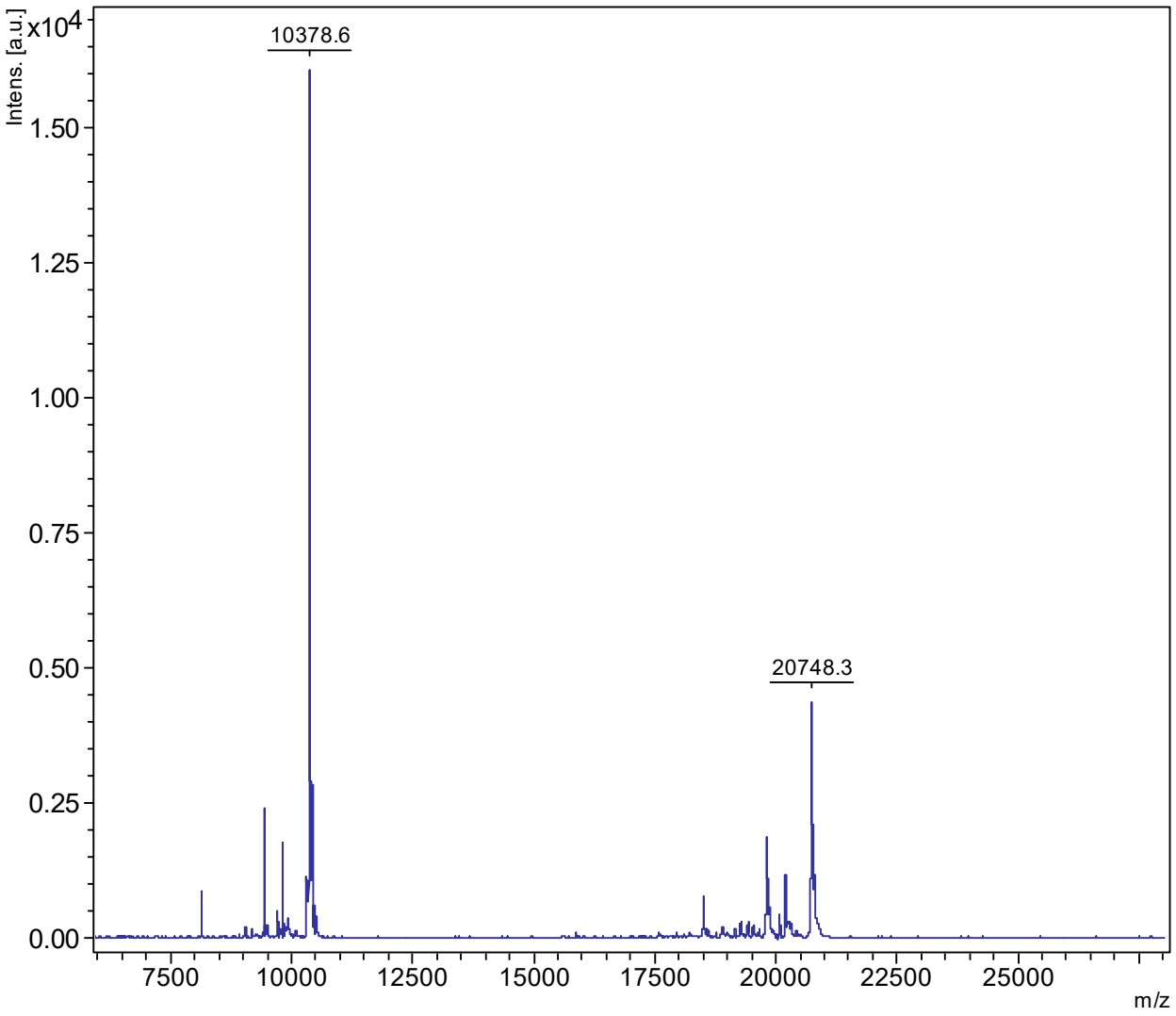

Figure S35. MALDI-TOF analysis of fully biotinylated G3 PAMAM dendrimer **7**.

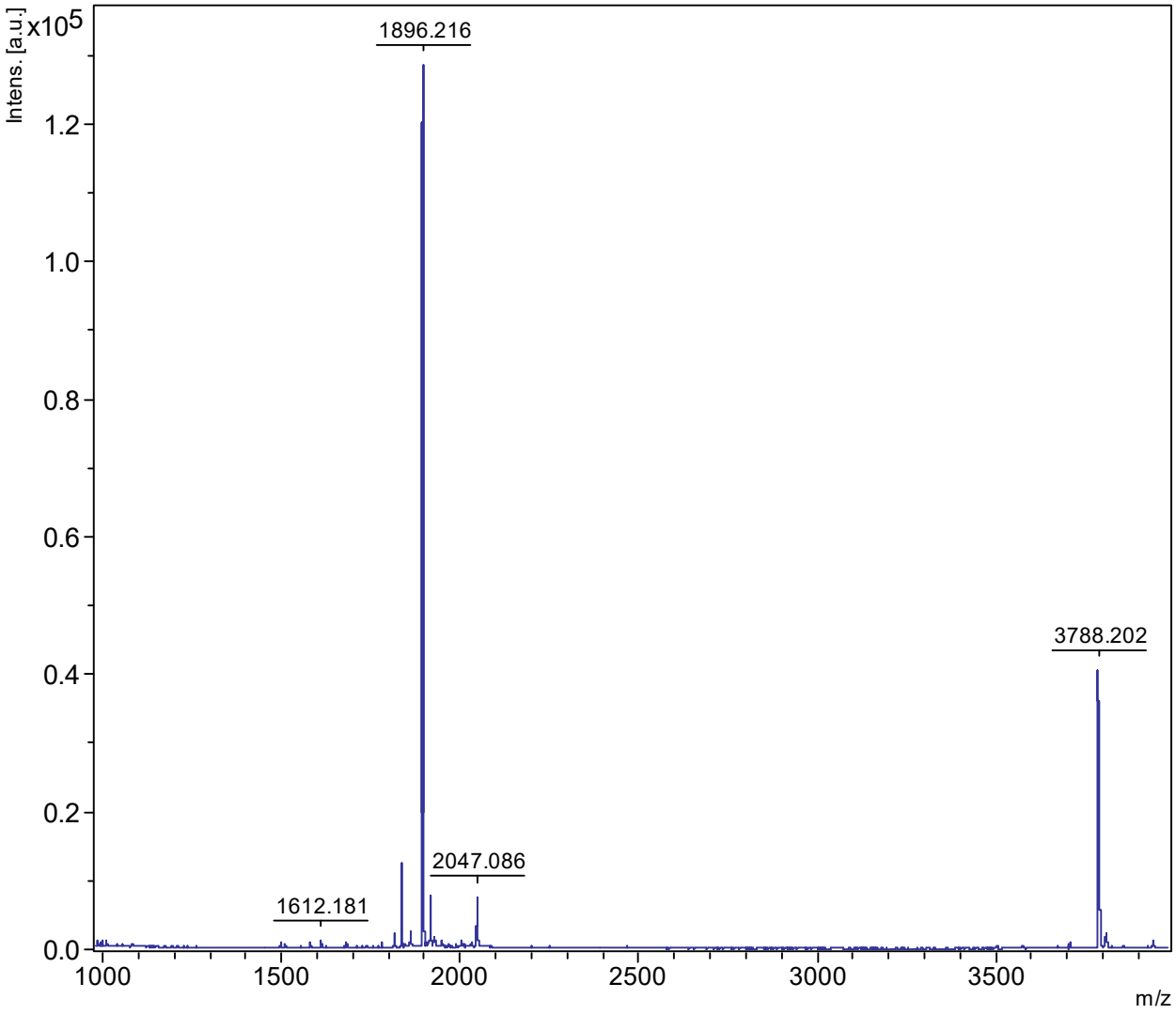

Figure S36. MALDI-TOF analysis of fully alkynylated G1-PAMAM dendrimer **8**.

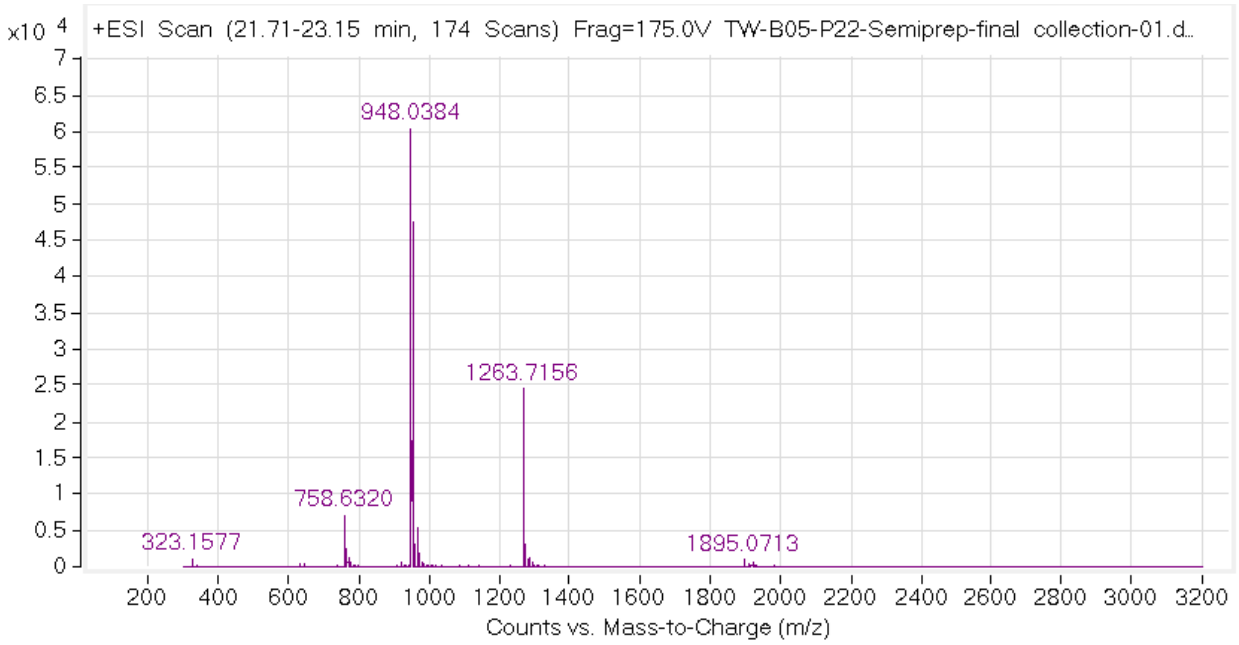

Figure S37. LC-UV-TOF analysis of fully alkynylated G1-PAMAM dendrimer **8**.

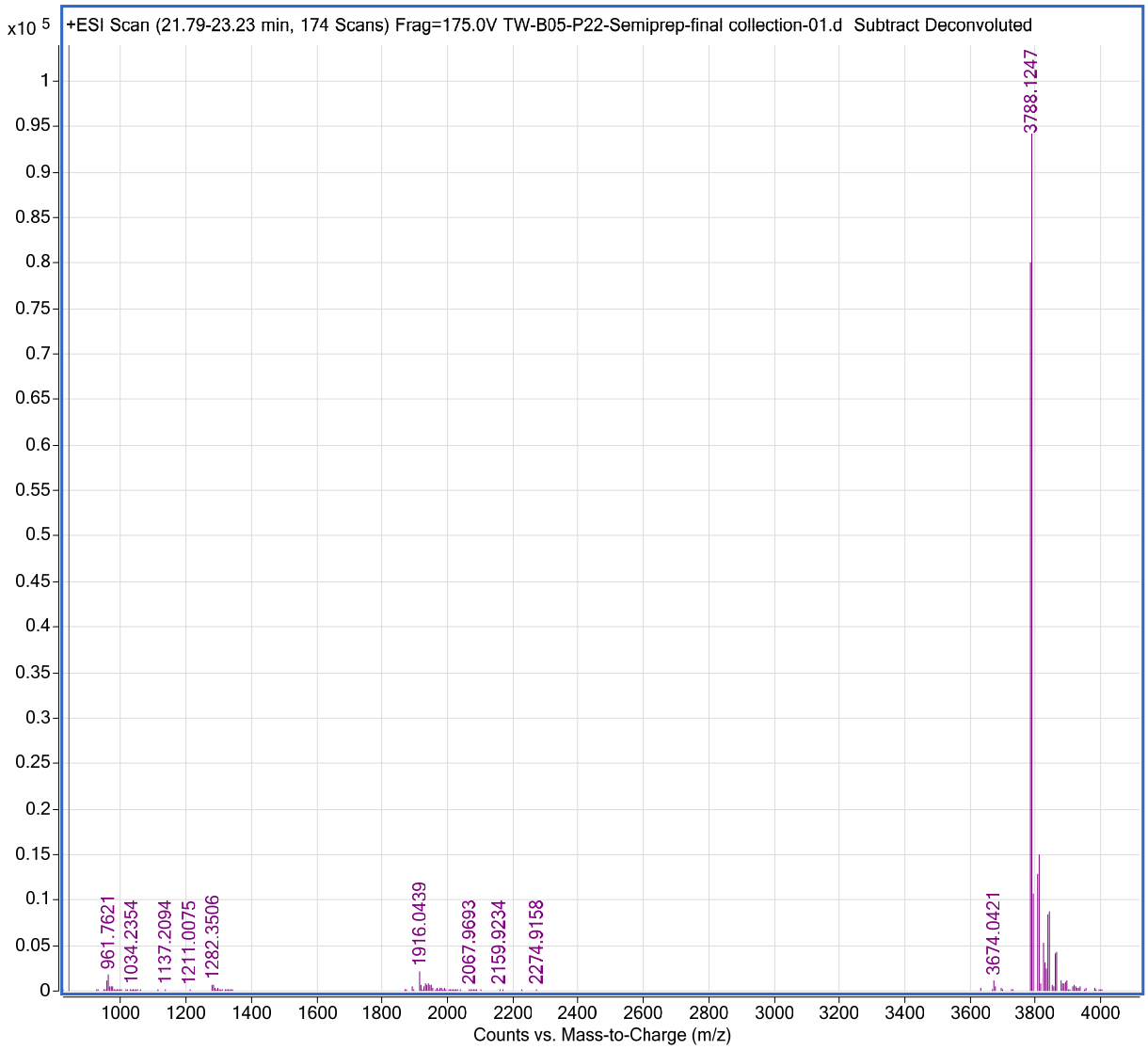

Figure S38. LC-TOF deconvolution result for fully alkynylated G1-PAMAM dendrimer **8**.

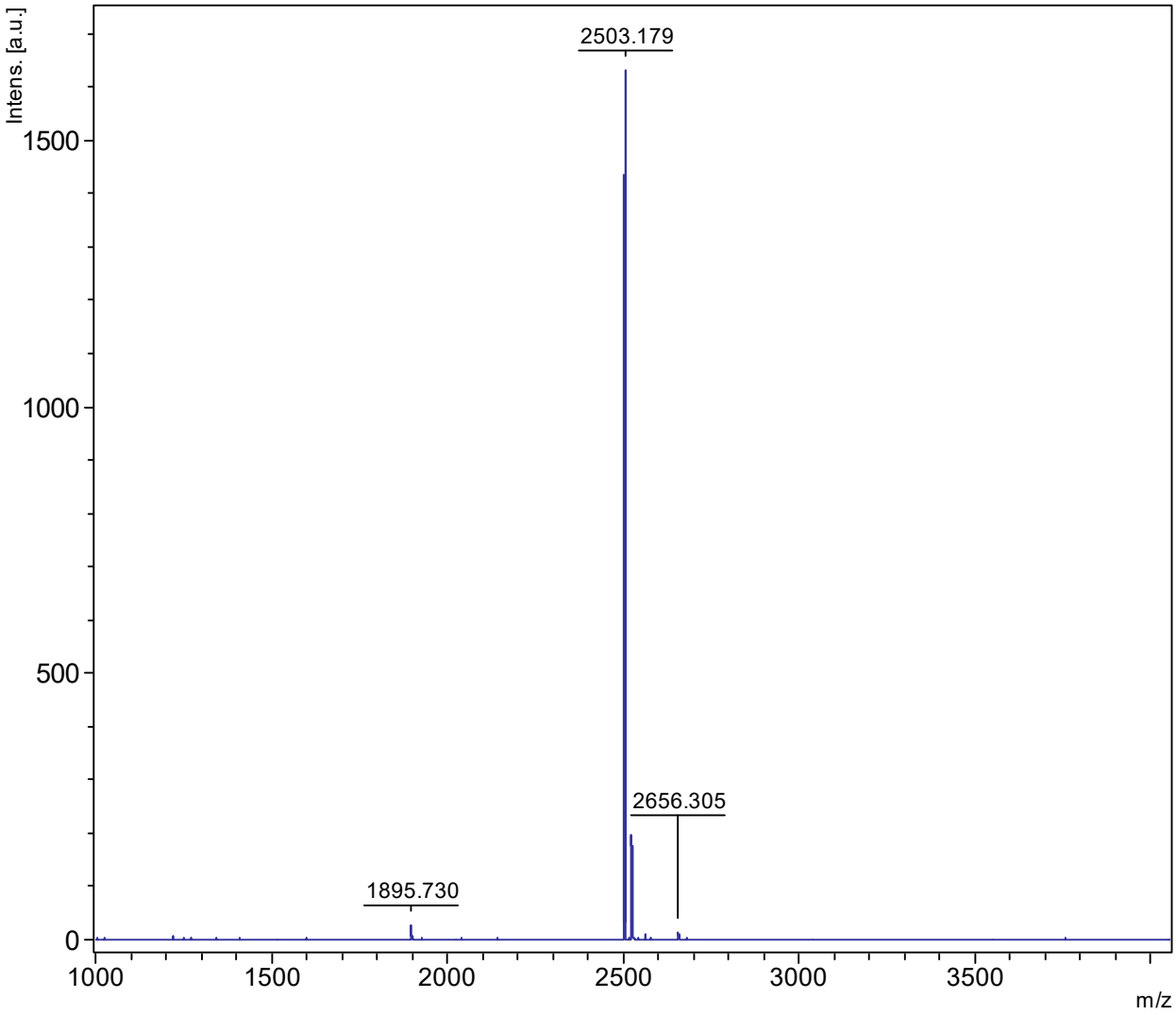

Figure S39. MALDI-TOF analysis of G1-PAMAM half-dendron-linker **12**.

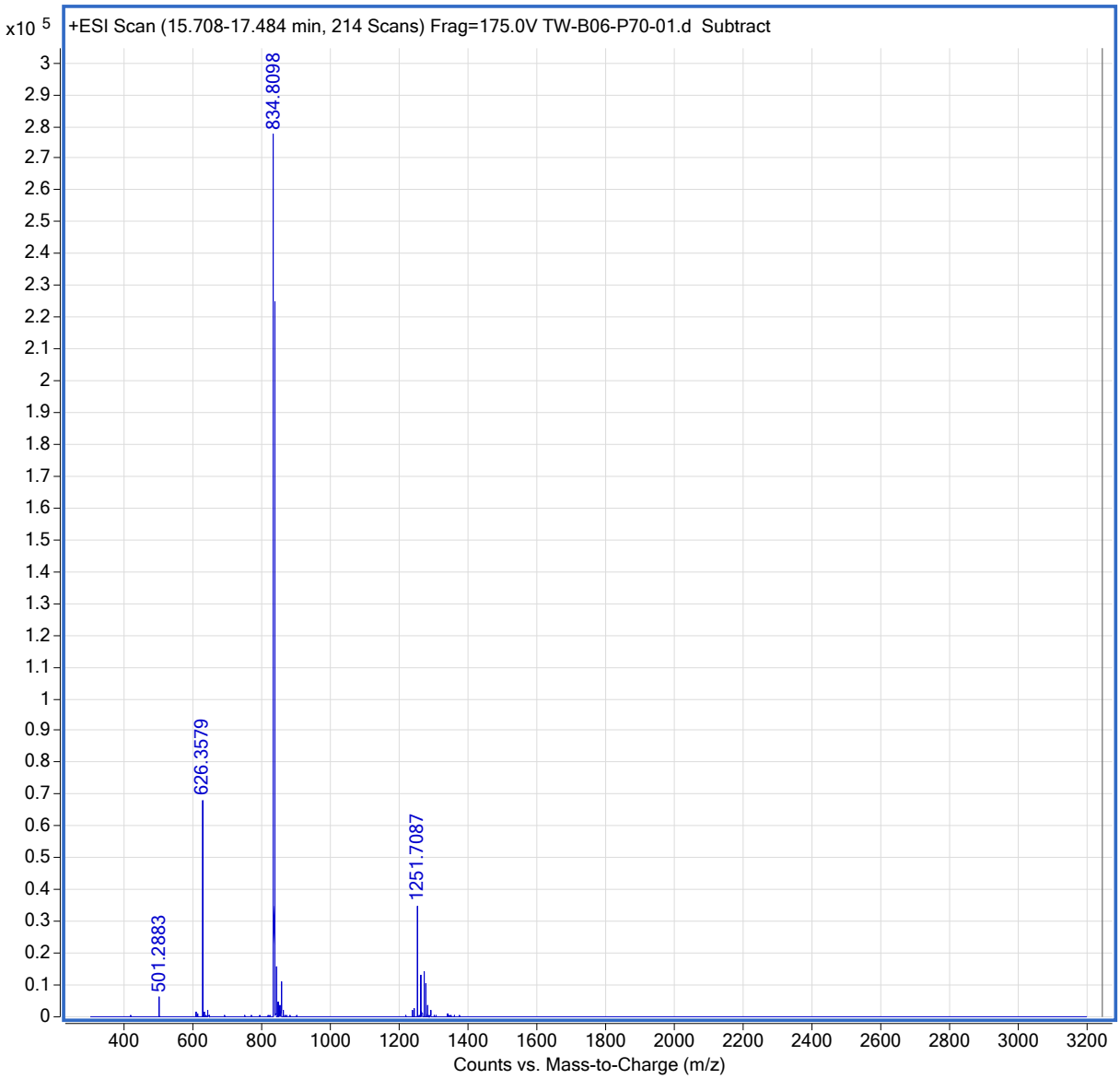

Figure S40. LC-UV-TOF analysis of G1-PAMAM half-dendron-linker **12**.

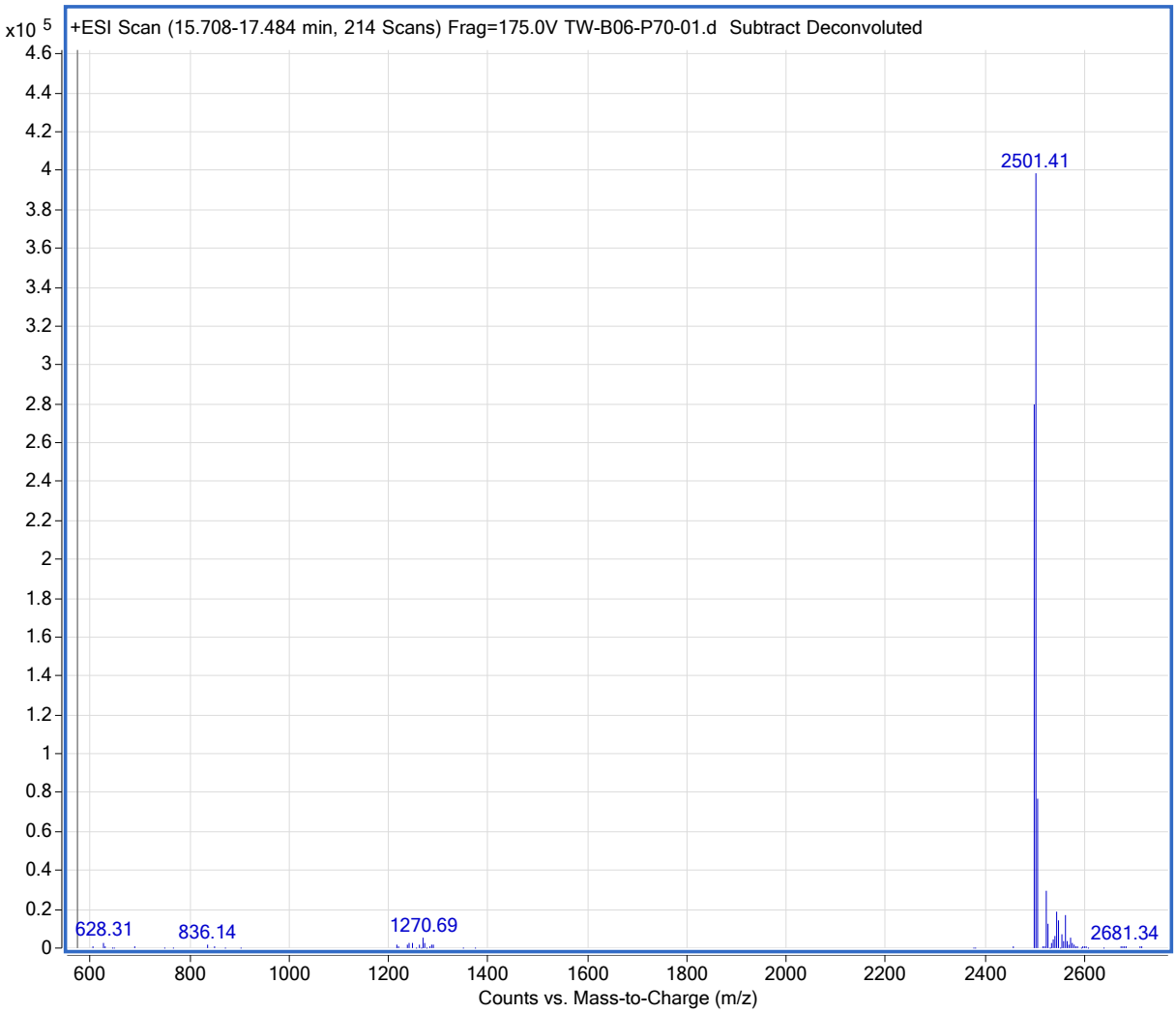

Figure S41. LC-UV-TOF deconvolution result for G1-PAMAM half-dendron-linker **12**.

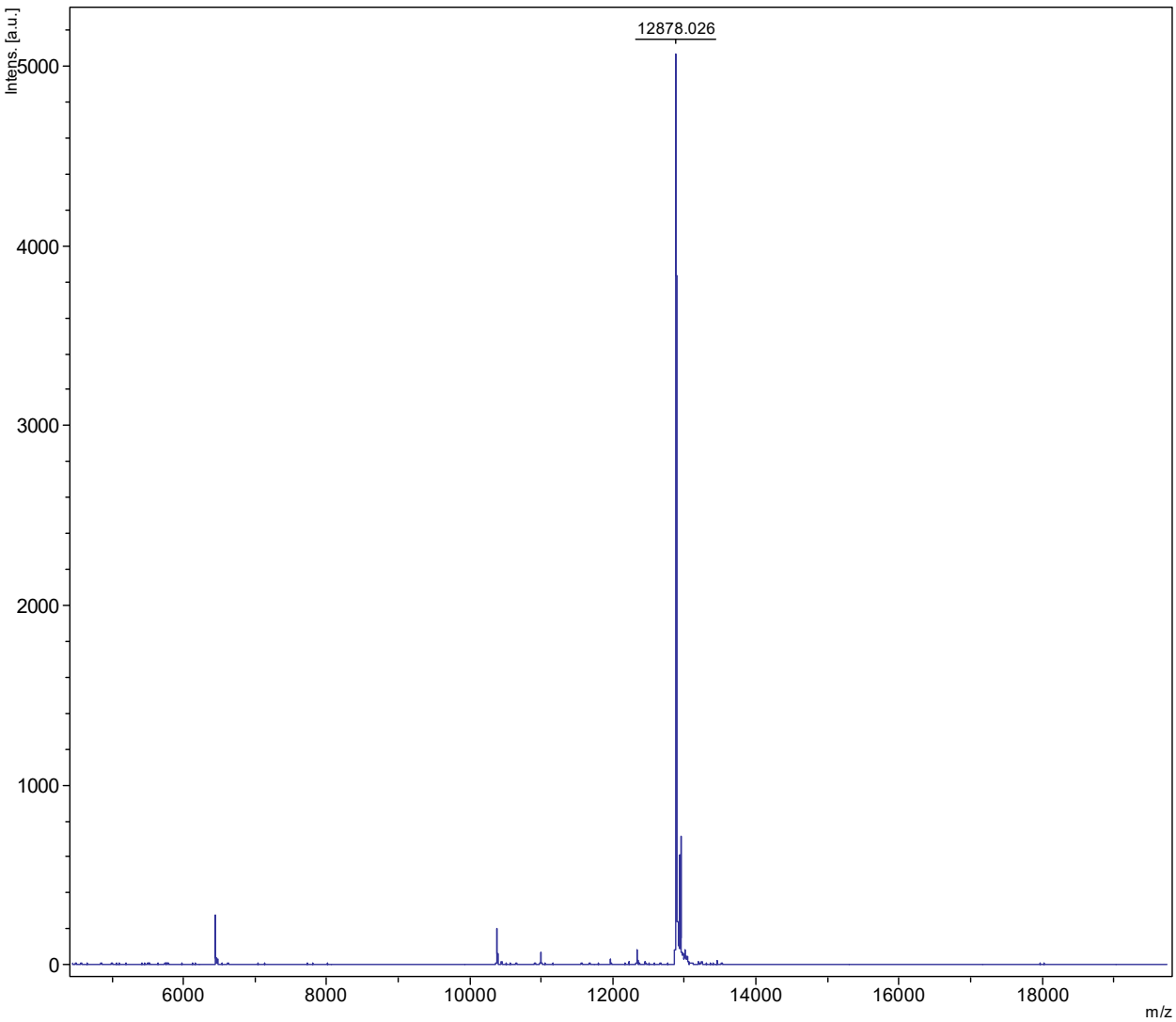

Figure S42. MALDI-TOF analysis of (G1 half-dendron)-linker-(G3 half-dendron) **6**.

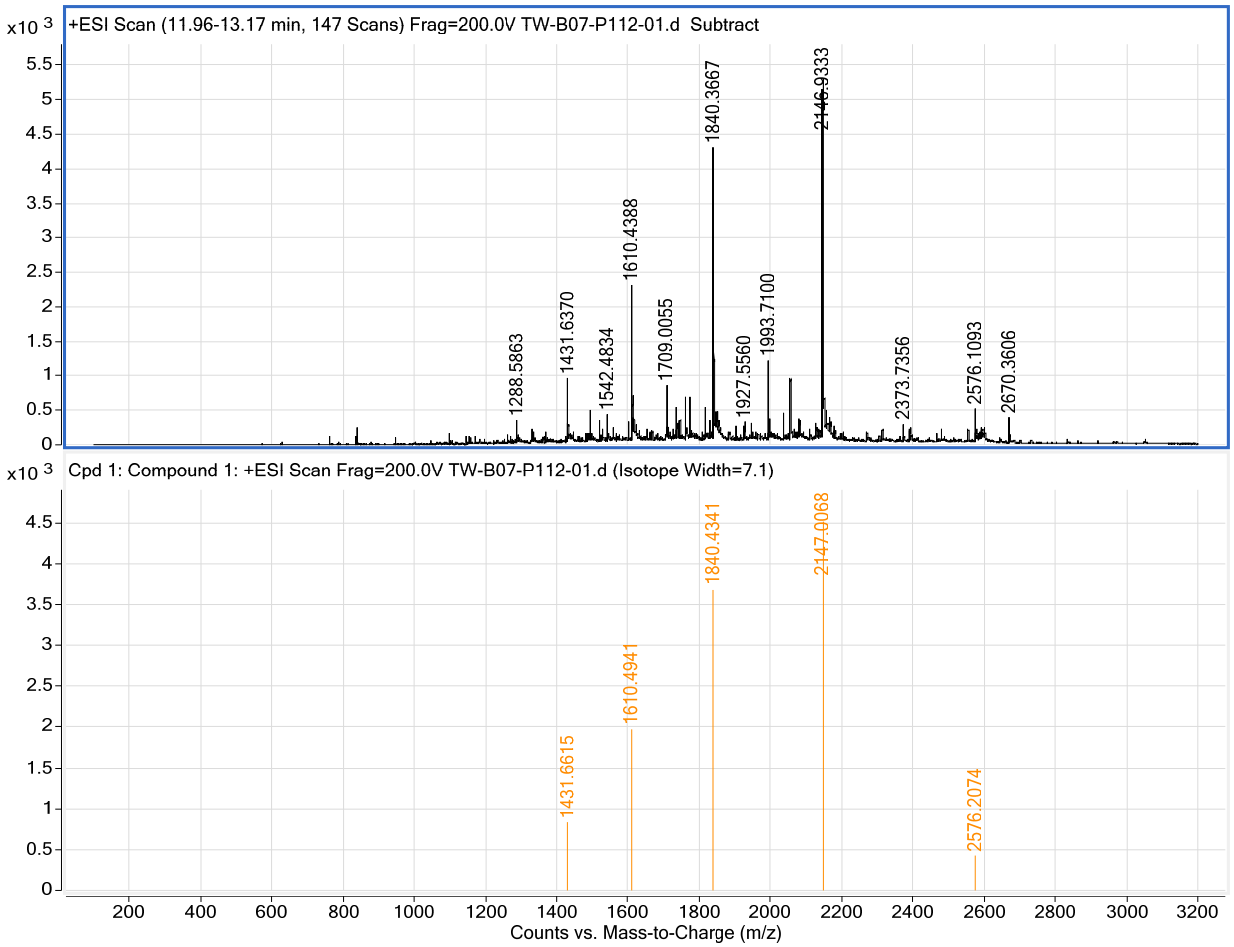

Figure S43. LC-UV-TOF mass analysis of (G1 half-dendron)-linker-(G3 half-dendron) **6**.

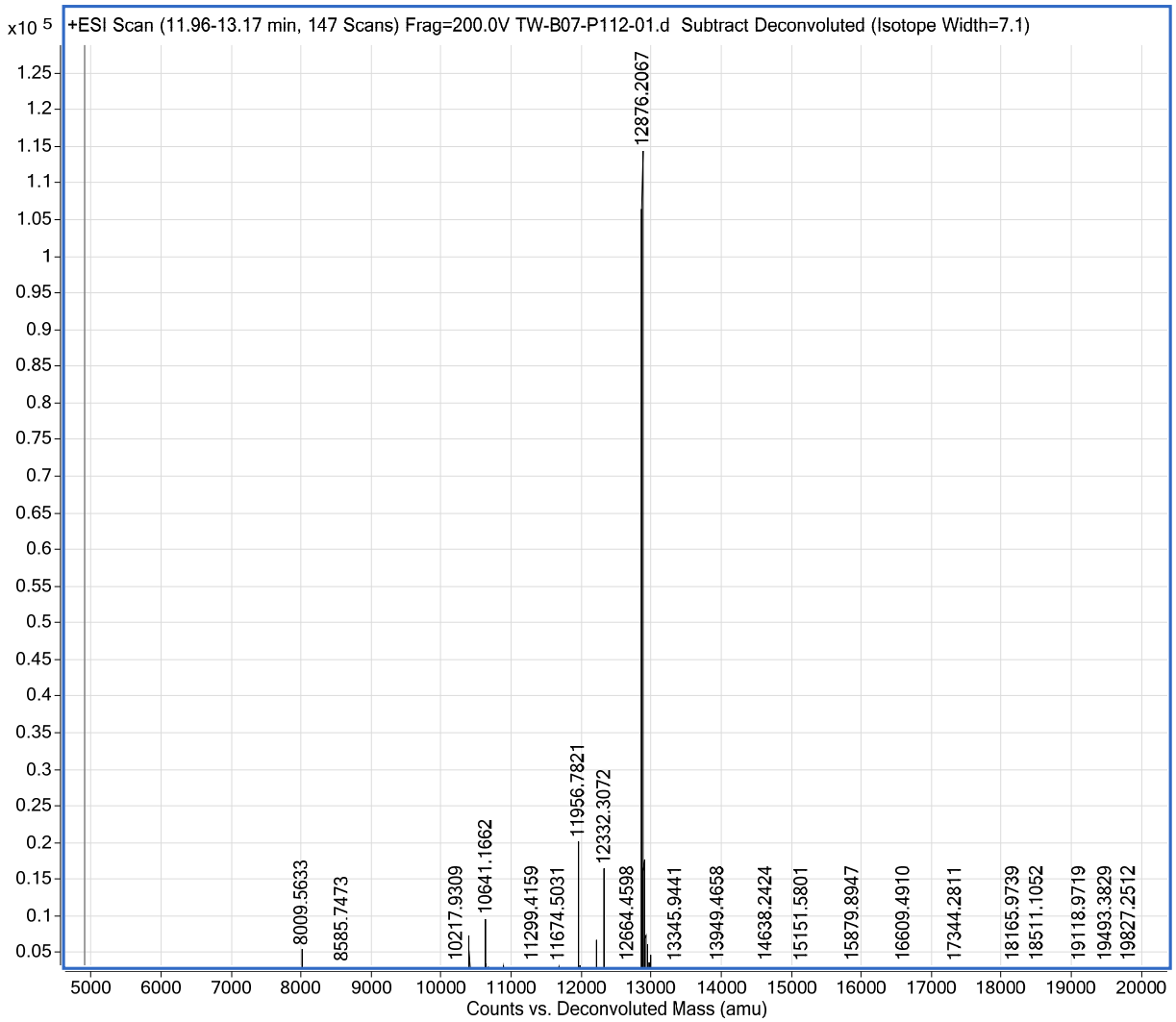

Figure S44. LC-UV-TOF deconvolution result of (G1 half-dendron)-linker-(G3 half-dendron) **6**.

(A)

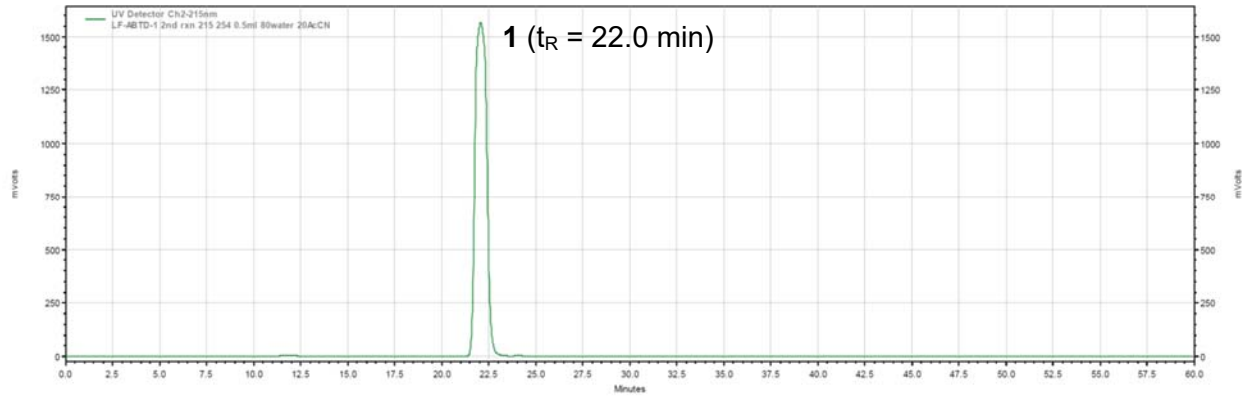

(B)

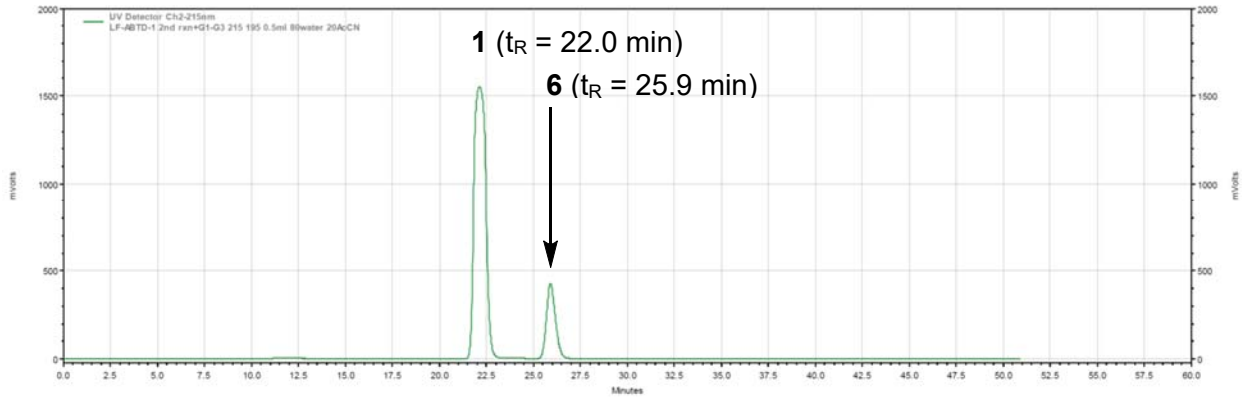

Figure S45. GPC analysis of (A) ABTD-TTC-1 (**1**) and (B) ABTD-TTC-1 (**1**) + click-ready ABTD **6**. Conditions: Ultrahydrogel™ 500 column (7.8 mm x 300 mm, 10 μm); MeCN/H_2O (20/80); 0.5 mL/min; 55 μM; UV detector at 215 nm.

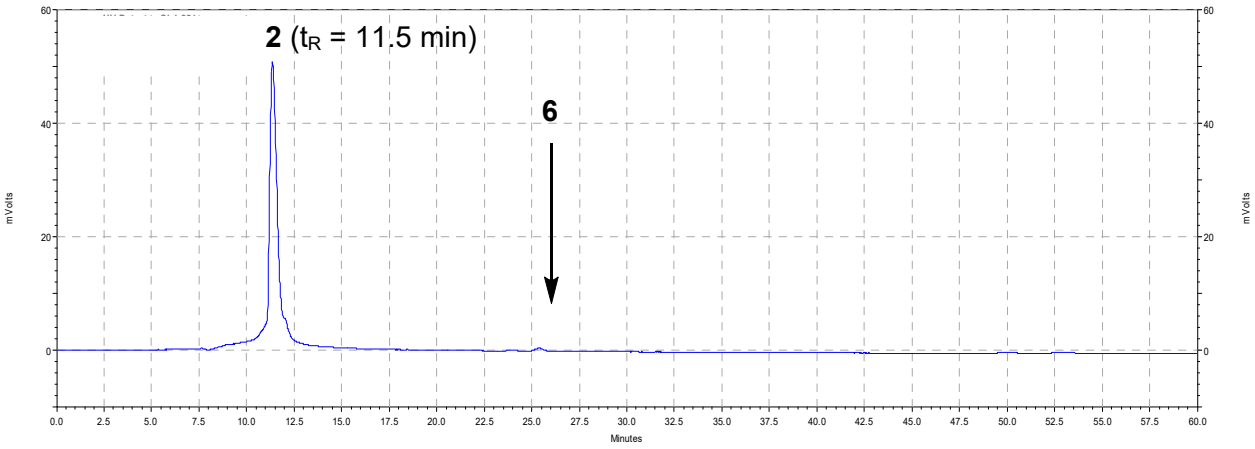

Figure S46. GPC analysis of ABTD-TTC-2 (**2**). Conditions: Ultrahydrogel^{TM} 500 column (7.8 mm x 300 mm, 10 μm); MeCN/H_2O (20/80); 0.5 mL/min; 50 μM; UV detector at 254 nm. The anticipated t_R of **6** is also shown.

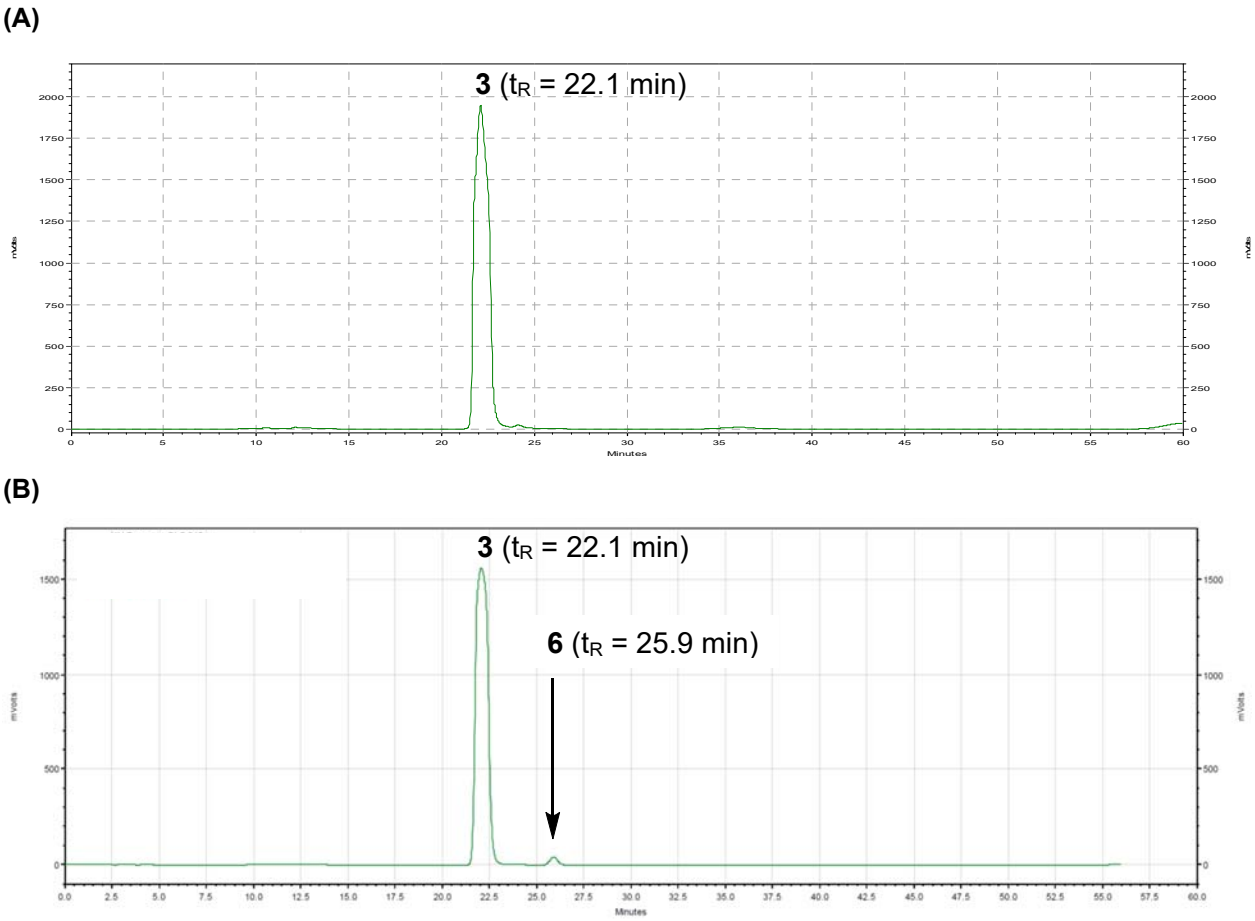

Figure S47. GPC analysis of (A) ABTD-TTC-3 (**3**) and (B) ABTD-TTC-2 (**2**) + click-ready ABTD **6**. Conditions: Ultrahydrogel^{TM} 500 column (7.8 mm x 300 mm); MeCN/H_2O (20/80); 0.5 mL/min; 64 μM; UV detector at 215 nm.

(A)

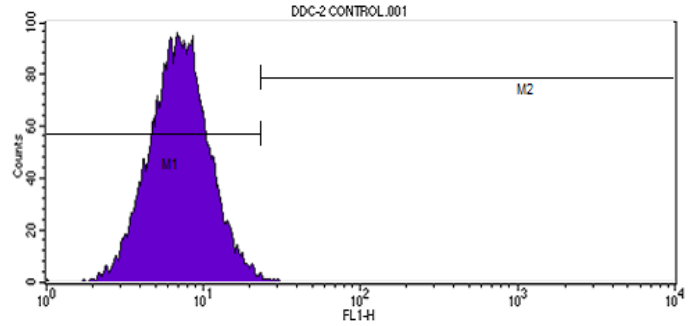

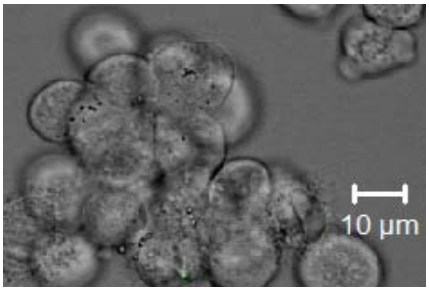

(B)

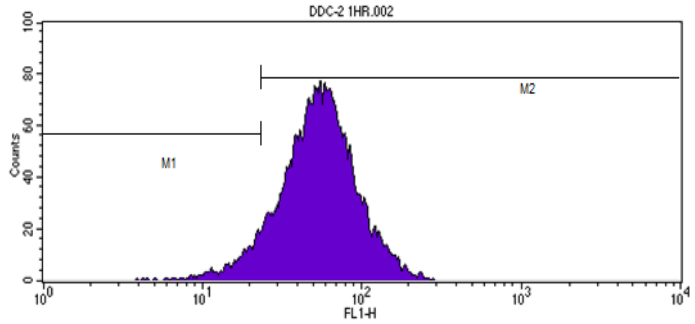

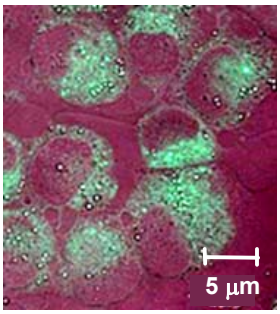

Figure S48. Internalization of fluorescent probe ABTD-TTC-2 (**2**) (20 µM) in ID-8 (ovarian cancer) cells by confocal fluorescence microscopy (CFM) and flow cytometry after 1 h of incubation at 37 °C (B) as compared to the control ID8 cells (A).

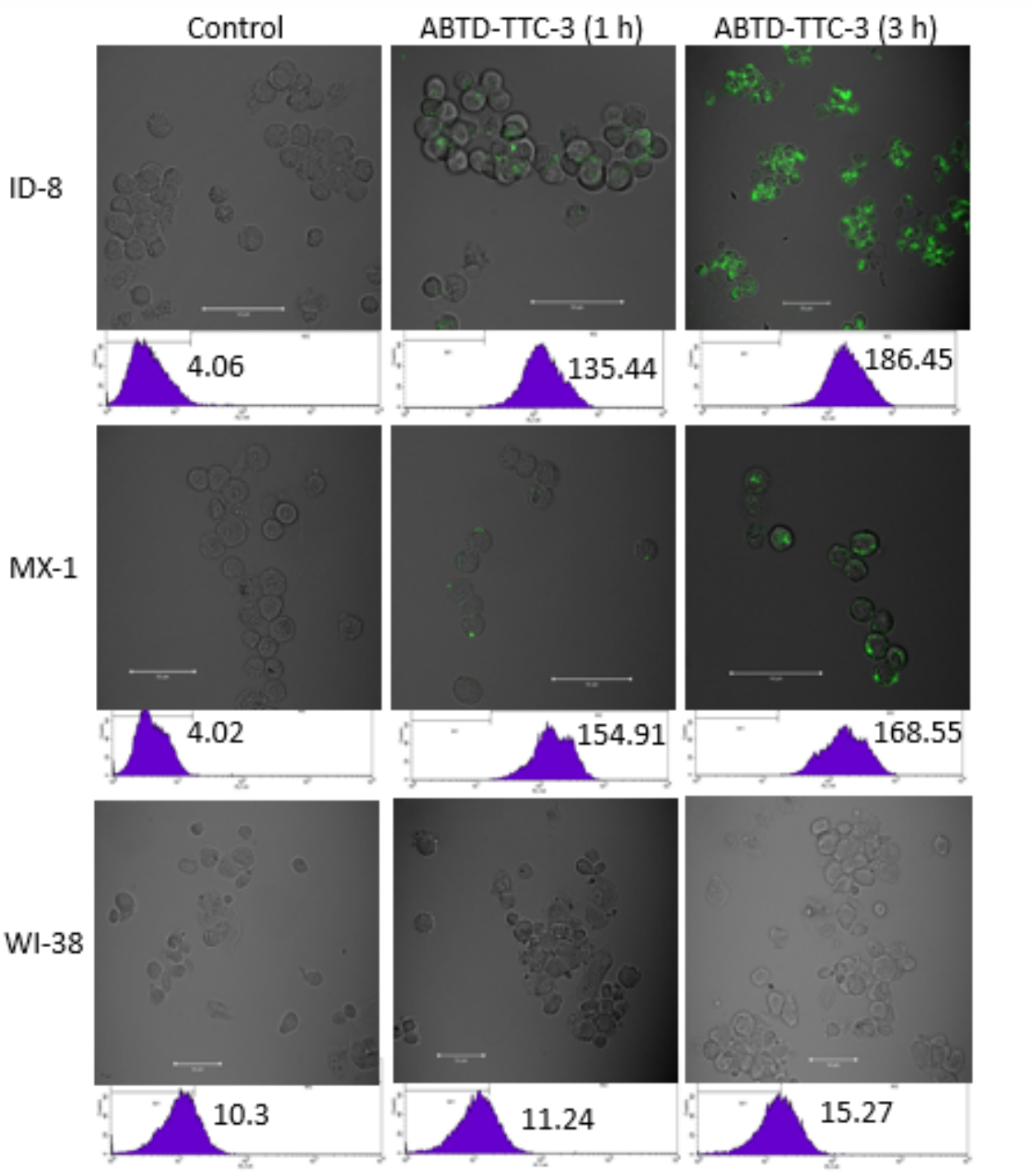

Figure S49. Assessment of the internalization of fluorescent probe ABTD-TTC-3 (**3**) (20 μM) in ID-8 (ovarian cancer), MX-1 (breast cancer) and WI-38 (normal lung fibroblast) cells by confocal fluorescence microscopy (CFM) and flow cytometry at 0 h, 1 h, and 3 h periods, at 37 °C.

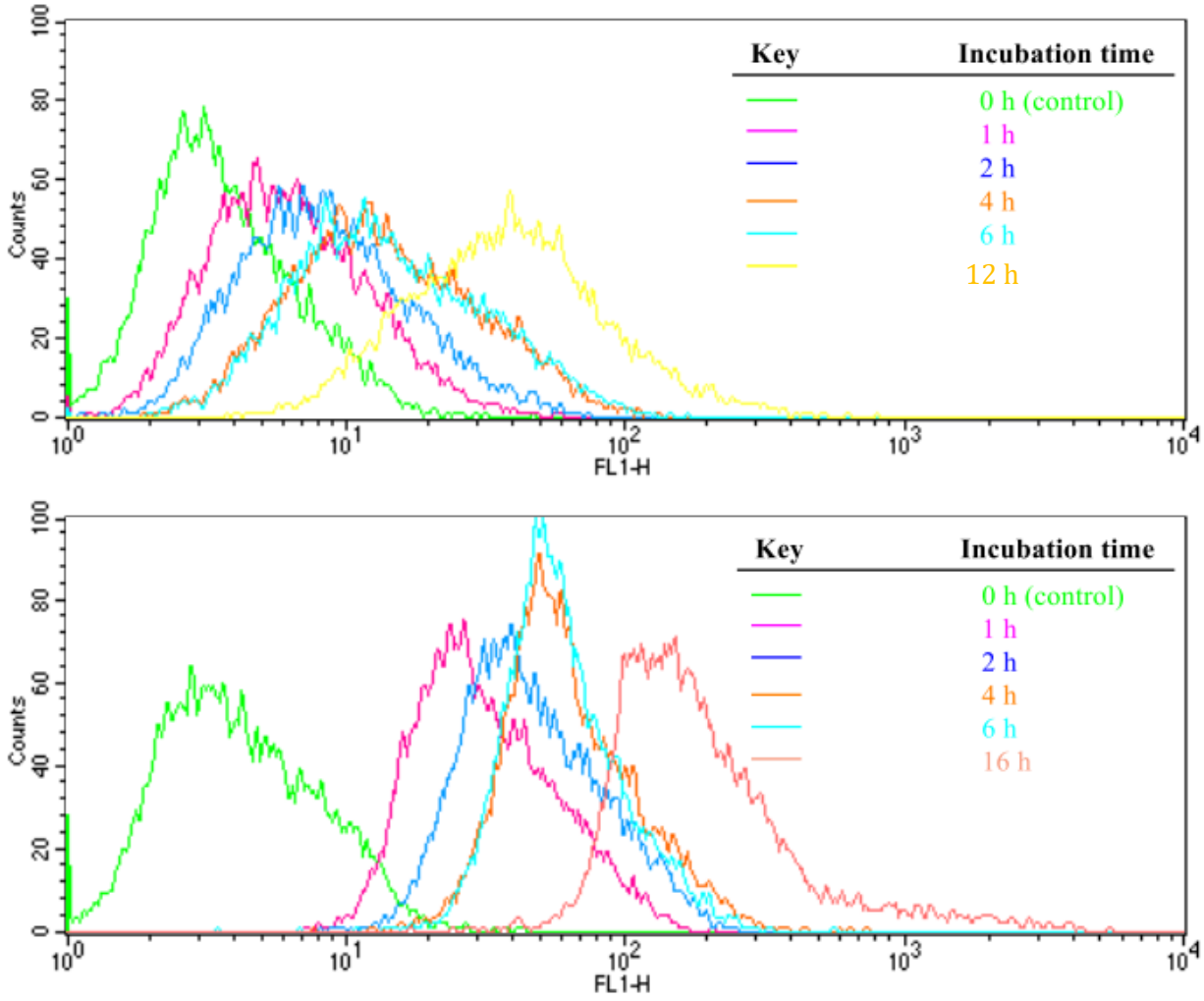

Figure S50. Assessment of the multi-binding effect by flow cytometry based on the internalization of fluorescent probe **28** (10 μM, top) and ABTD-TTC-3 (**3**) (10 μM, bottom) in ID-8 cells at 0, 1, 2, 4, 6 and 16 h periods, at 37 °C.

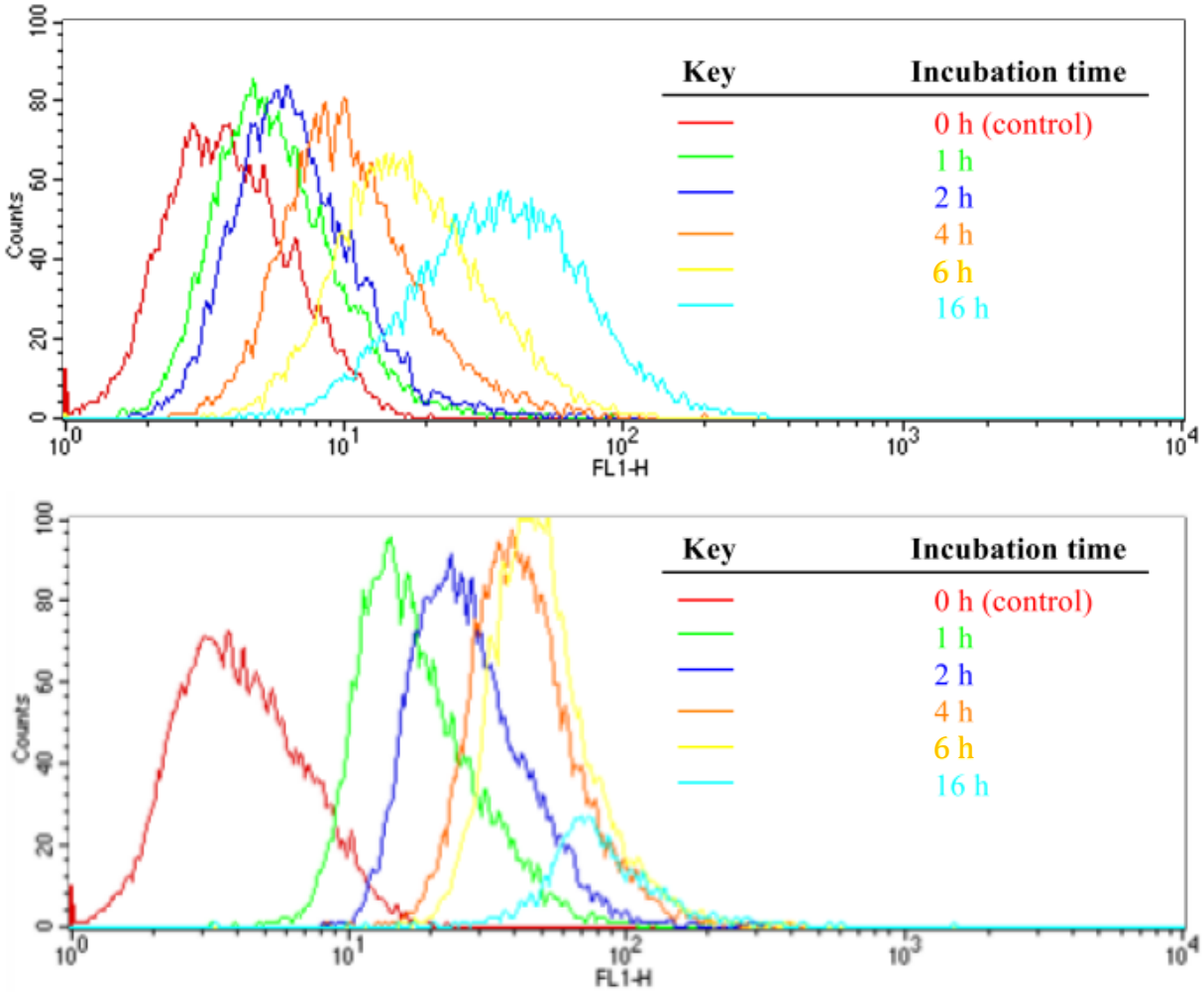

Figure S51. Assessment of the multi-binding effect by flow cytometry based on the internalization of fluorescent probe **28** (10 µM, top) and ABTD-TTC-3 (**3**) (10 µM, bottom) in MX-1 cells at 0, 1, 2, 4, 6 and 16 h periods, at 37 °C.